Physics Letters B 738 (2014) 97–108

Contents lists available at ScienceDirect

Physics Letters B

www.elsevier.com/locate/physletb

Beauty production in pp collisions at $\sqrt{s} = 2.76$ TeV measured via semi-electronic decays

ALICE Collaboration *

ARTICLE INFO

Article history:
Received 29 May 2014
Received in revised form 14 August 2014
Accepted 10 September 2014
Available online 17 September 2014
Editor: L. Rolandi

Keywords:
LHC
ALICE experiment
pp collisions
Single electrons
Heavy-flavour production
Beauty production

ABSTRACT

The ALICE Collaboration at the LHC reports measurement of the inclusive production cross section of electrons from semi-leptonic decays of beauty hadrons with rapidity $|y| < 0.8$ and transverse momentum $1 < p_{\mathrm{T}} < 10$ GeV/c, in pp collisions at $\sqrt{s} = 2.76$ TeV. Electrons not originating from semi-electronic decay of beauty hadrons are suppressed using the impact parameter of the corresponding tracks. The production cross section of beauty decay electrons is compared to the result obtained with an alternative method which uses the distribution of the azimuthal angle between heavy-flavour decay electrons and charged hadrons. Perturbative QCD predictions agree with the measured cross section within the experimental and theoretical uncertainties. The integrated visible cross section, $\sigma_{\mathrm{b}\to\mathrm{e}} = 3.47 \pm 0.40(\mathrm{stat})^{+1.12}_{-1.33}(\mathrm{sys}) \pm 0.07(\mathrm{norm})$ μb, was extrapolated to full phase space using Fixed Order plus Next-to-Leading Log (FONLL) calculations to obtain the total $\mathrm{b\bar{b}}$ production cross section, $\sigma_{\mathrm{b\bar{b}}} = 130 \pm 15.1(\mathrm{stat})^{+42.1}_{-49.8}(\mathrm{sys})^{+3.4}_{-3.1}(\mathrm{extr}) \pm 2.5(\mathrm{norm}) \pm 4.4(\mathrm{BR})$ μb.

1. Introduction

Perturbative Quantum Chromodynamics (pQCD) calculations of the production of heavy (charm and beauty) quarks can be carried out with well-controlled accuracy, due to the hard (high Q^2) scale imposed by the large mass of heavy quarks [1–3]. In addition, the large mass implies that heavy quark production in high energy collisions of heavy ions occurs early compared to the formation time of the strongly interacting partonic matter generated in such collisions [4–7]. Therefore, the study of heavy quark production in pp collisions is of interest for two reasons: the measurement of their production cross section provides essential tests of pQCD, and such measurements yield the necessary reference for the corresponding measurements performed in heavy-ion collisions. Properties of the strongly interacting, partonic medium generated in high energy heavy-ion collisions are studied using various heavy-quark observables [8–11].

The ALICE Collaboration has reported heavy-flavour measurements in pp collisions at $\sqrt{s} = 2.76$ TeV for D meson production via hadronic decays at mid-rapidity [12], heavy-flavour hadron production via semi-leptonic decays to electrons (mid-rapidity) and muons (forward rapidity) [13,14], and J/ψ production using the di-muon (forward rapidity) and di-electron (mid-rapidity) decay channels [15]. All measurements are in good agreement with pQCD calculations for inclusive $q\bar{q}$ production, and with QCD-inspired models for J/ψ production. Since both charm and beauty hadrons decay semi-leptonically, the measured distribution of heavy-flavour decay muons and electrons have contributions from both.

The objective of the analyses presented here is to obtain the total beauty production cross section by measuring the p_{T}-differential inclusive production cross section of electrons from semi-electronic decays of beauty hadrons. The measurement is performed in the mid-rapidity region ($|y| < 0.8$) with the ALICE detector for $1 < p_{\mathrm{T}} < 10$ GeV/c, in pp collisions at $\sqrt{s} = 2.76$ TeV. The total $\mathrm{b\bar{b}}$ production cross section is determined by the extrapolation of the measured p_{T}-differential production cross section to full p_{T} and y ranges. The measured relative beauty contribution to the heavy-flavour decay electrons and the inclusive production cross section of electrons from semi-electronic decays of beauty hadrons are compared to the predictions from three different pQCD calculations (FONLL [1], GM-VFNS [16], and k_{T}-factorization [3]). The primary analysis presented here uses a track impact parameter discriminant, which takes advantage of the relatively long lifetime of beauty hadrons ($c\tau \sim 500$ μm) compared to charm hadrons. A second method discriminates beauty from charm production using the distribution of the azimuthal angle between heavy-flavour decay electrons and charged hadrons, $\Delta\varphi$. For beauty hadron decays the width of the near-side peak, $\Delta\varphi$ around zero, is indeed larger than that of charm hadron decays, due to the decay kinematics of the heavier mass beauty hadrons. The difference is exploited to measure the relative beauty contribution to the heavy-flavour decay electron population, which can

* alice-publications@cern.ch.

http://dx.doi.org/10.1016/j.physletb.2014.09.026

be used along with the measured heavy-flavour electron spectrum to compute the production cross section of electrons from beauty hadron decays.

2. Event and track selection

The data set used for these analyses was recorded during the 2011 LHC run with pp collisions at $\sqrt{s} = 2.76$ TeV. The Minimum Bias (MB) collisions were triggered using the V0 scintillator detectors, located in the forward ($2.8 < \eta < 5.1$) and backward ($-3.7 < \eta < -1.7$) regions, and the Silicon Pixel Detector (SPD), which is the innermost part of the Inner Tracking System (ITS). The SPD consists of two cylindrical layers of hybrid silicon pixel assemblies, covering a pseudo-rapidity interval $|\eta| < 2.0$ and $|\eta| < 1.4$ for the inner and outer layer, respectively. Both the V0 and SPD detectors cover the full azimuth. The MB trigger required at least one hit in either of the V0 scintillator detectors or in the SPD, in coincidence with the presence of an LHC bunch crossing. Additional details can be found in [12]. The MB trigger cross section was measured to be 55.4 ± 1.0 mb using a van der Meer scan [17]. A fraction of MB events were triggered independently of the read-out state of the Silicon Drift Detector (SDD), which equips the two intermediate layers of the ITS. The Electromagnetic Calorimeter (EMCal) is a sampling calorimeter based on Shashlik technology, covering a pseudo-rapidity interval $|\eta| < 0.7$ and covering 100° in azimuth [18]. The EMCal Single Shower (SSh) trigger system generates a fast energy sum (800 ns) at Trigger Level 0 for overlapping groups of 4×4 ($\eta \times \varphi$) adjacent EMCal towers, followed by comparison to a threshold energy [19]. The data set recorded with the EMCal trigger required that the MB trigger condition was fulfilled, and that at least one SSh sum exceeded a nominal threshold energy of 3.0 GeV. The results reported are based on 51.5 million MB events (integrated luminosity of 0.9 nb^{-1}) and 0.64 million EMCal triggered events (integrated luminosity of 14.9 nb^{-1}). The impact parameter analysis was performed solely on the MB sample. The method based on the distribution of the azimuthal angle between heavy-flavour decay electrons and charged hadrons (i.e. electron–hadron correlation) was done using both the MB and EMCal trigger samples. In the offline analysis, events which satisfied the trigger conditions were required to have a collision vertex with at least two tracks pointing to it and the vertex position along the beam line to be within ±10 cm of the nominal centre of the ALICE detector.

Charged particle tracks were reconstructed offline using the Time Projection Chamber (TPC) [20] and the ITS [21]. To have a homogeneously reconstructed sample of tracks, the SDD points were always excluded from the track reconstruction used for these analyses. EMCal clusters were generated offline via an algorithm that combines signals from adjacent EMCal towers. The cluster size was constrained by the requirement that each cluster contains only one local energy maximum. In the case of the EMCal-based analysis, charged tracks were propagated to the EMCal and matched to clusters in the EMCal detector. The matching required the difference between the cluster position and track extrapolation at the EMCal surface to be smaller than 0.025 units in η and 0.05 radians in φ.

Electrons were identified using the TPC, Time of Flight (TOF), and EMCal detectors [13]. Background hadrons, in particular charged pions, were rejected using the specific energy loss, $\mathrm{d}E/\mathrm{d}x$, of charged particles measured in the TPC. Tracks were required to have a $\mathrm{d}E/\mathrm{d}x$ value between one standard deviation below and three standard deviations above the expected value for electrons. In the low momentum region (below 2.0 GeV/c for the impact parameter analysis and below 2.5 GeV/c for the correlation analysis) electron candidates were required to be consistent within three standard deviations with the electron time of flight hypothesis. TOF-based discrimination is not efficient at higher transverse momentum and the TOF was not required. The EMCal-based correlation analysis required E/p to be within a window of 0.8 and 1.2 times the nominal value of E/p for electrons, where E is the energy deposited in the EMCal and p is the track momentum measured in the tracking system. Tracks were required to have hits in the SPD in order to suppress the contribution of electrons that originated from photon conversions in the inner tracking detector material and to improve the resolution on the track impact parameter.

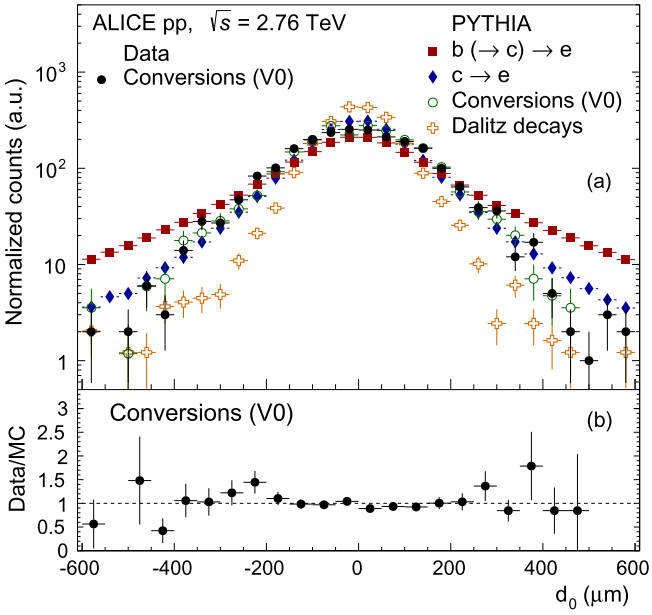

Fig. 1. (Colour online.) (a) Transverse impact parameter (d_0) distributions of electrons from beauty and charm hadron decays, light hadron decays, and photon conversions obtained with PYTHIA 6 simulations in the electron p_T range $1 < p_T < 6$ GeV/c, along with the measured distribution of conversion electrons. The distributions are normalized to the same integrated yield. (b) Ratios of the measured and simulated d_0 distributions of conversion electrons in the ranges $1 < p_T < 6$ GeV/c.

3. Analysis

3.1. Impact parameter technique

The measured electron sample contains contributions from beauty and charm hadron decays, along with background sources. The background is primarily composed of electrons from photon conversions in the beam-pipe and ITS material, π^0 and η Dalitz decays, and di-electron decays of light neutral vector mesons. The relative contribution of electrons from beauty hadron decays can be enhanced by selecting on the displacement of electron tracks from the primary vertex of the pp collision, as described in detail in [22].

The relatively long lifetime of beauty hadrons was exploited by selecting on the transverse impact parameter (d_0), which is the projection of the charged track distance of closest approach to the primary vertex vector onto the transverse plane, perpendicular to the beam line. The sign of d_0 is given according to the track position relative to the primary vertex after the track has been spatially extended in the direction perpendicular to its p_T vector. The resolution of d_0 is better than 85 μm for $p_T > 1$ GeV/c. Fig. 1(a) shows the impact parameter distribution for all significant contributions to the measured electron sample in the range $1 < p_T < 6$ GeV/c. The distributions were obtained using a Monte Carlo (MC) simulation with GEANT3 [23], where the pp collisions were produced using the PYTHIA 6 event generator (Perugia-0 tune) [24]. Each

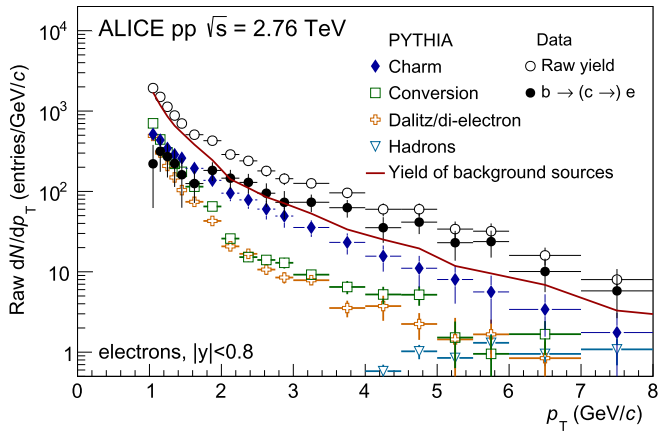

Fig. 2. (Colour online.) Raw spectrum of electrons from the impact parameter analysis (open circles) compared to background sources (from charm hadron decays, photon conversions, Dalitz decays, and hadron contamination) as a function of p_T. The background sources originating from light flavour hadrons were obtained using a MC simulation and reweighted according to the π^0 p_T spectrum measured with ALICE [25]. The charm hadron decay background was estimated using the charm hadron spectra measured with ALICE [26]. The raw yield after background sources are subtracted is also shown (filled circles). The error bars represent the statistical uncertainties.

source has a distinct d_0 distribution. The d_0 distribution of electrons from Dalitz decays is relatively narrow compared to that from beauty hadron decays, since Dalitz electrons are effectively generated at the collision vertex. The charm hadron decay and conversion electron d_0 distributions are broader than that of the Dalitz decay distribution since they emerge from secondary vertices, but are not as broad as those from beauty decays. For comparison, the d_0 distribution of conversion electrons from data is also shown in the figure. This pure sample of electrons from photon conversions in the detector material was identified using a V0-finder and an optimized set of topological selection requirements. Fig. 1(b) shows the ratio of the impact parameter distribution from data to that from simulation in the range $1 < p_T < 6$ GeV/c. The ratio is close to unity, showing good agreement of the simulation and measurement of photon conversion electron candidates.

A selection on the transverse impact parameter d_0 was applied in order to maximize the signal to background (S/B) ratio of electrons from beauty hadron decays. The requirement on the minimum impact parameter is p_T dependent, since the width of the d_0 distribution depends on p_T. The S/B ratio varies with p_T due to different impact parameter selection efficiency for the various sources. Therefore, separate p_T-dependent parameterizations of the d_0 selection requirement were obtained for the analyses which utilize TPC-TOF and TPC-only for electron selection. Electron candidates accepted for the TPC-TOF analysis satisfied the condition $|d_0| > 64 + 480 \cdot \exp(-0.56 p_T)$ (with d_0 in μm and p_T in GeV/c), while $|d_0| > 54 + 780 \cdot \exp(-0.56 p_T)$ was required for the TPC-only analysis.

The raw p_T distribution of electrons, after the application of track selection criteria, is shown in Fig. 2, along with the p_T distributions of electrons from the various background sources (charm hadron decays, photon conversions, Dalitz/di-electron decays, and hadron contamination). The background distributions were obtained from a MC simulation, with GEANT3. The p_T distributions of the background sources were normalized to the total number of events which passed the event selection requirements, and were corrected for the efficiency to reconstruct a primary collision vertex. Among all background contributions, Dalitz decay electrons and photon conversions are dominant at low p_T, where more than 80% of the background can be attributed to π^0 Dalitz decays and conversions of photons from π^0 decays. At high p_T the contribution from charm hadron decays is significant. The contribution from heavy quarkonia decays also becomes significant at high p_T, although this contribution is strongly suppressed in the analysis since the selection on d_0 strongly suppresses tracks from such decays. The PYTHIA simulation does not precisely reproduce the p_T-differential spectra of background sources measured in data. Therefore, the sources of background electrons simulated with PYTHIA were reweighted according to the π^0 p_T spectrum measured with ALICE [25] and were then propagated in the ALICE apparatus using GEANT3. The spectra of other light mesons were estimated via m_T-scaling of the π^0 spectrum. The electron background from charm hadron decays was estimated based on the charm hadron spectra measured with ALICE. The D meson production cross sections were obtained by applying a $\sqrt{s}$ scaling to the cross sections measured at $\sqrt{s} = 7$ TeV [26]. The scaling factor was defined as the ratio of the cross sections from the FONLL calculations at 2.76 and 7 TeV. The theoretical uncertainty on the scaling factor was evaluated by varying quark mass and the perturbative scales as described in [27]. The D meson production cross sections were measured with ALICE, with limited precision and p_T coverage, in pp collisions at $\sqrt{s} = 2.76$ TeV [12]. These measurements were found to be in agreement with the scaled 7 TeV measurements within statistical uncertainties. A contribution from Λ_c decays was included using the measured ratio $\sigma(\Lambda_c)/\sigma(D^0 + D^+)$ from ZEUS [28]. The background electrons surviving the selection criteria, including the condition on d_0, were subtracted from the measured electron distribution. Hadron contamination was estimated using a simultaneous fit of the electron and the different hadron components of the TPC dE/dx distribution in momentum slices. The contamination was negligible below 4 GeV/c but is significant at higher momenta. At 8 GeV/c it was found to be approximately 7%. The contamination was statistically subtracted from the measured electron distribution. The resulting p_T distribution is shown as filled circles in Fig. 2.

The electron yield from beauty hadron decays was corrected for geometrical acceptance, track reconstruction efficiency, electron identification efficiency, and efficiency of the d_0 cut. The invariant cross section of inclusive electron production from beauty hadron decays in the range $|y| < 0.8$ was then calculated using the corrected electron p_T spectrum, the number of MB pp collisions and the MB cross section. The details are described in [22].

To evaluate systematic uncertainties, the analysis was repeated with modified track selection and Particle IDentification (PID) criteria. The contributions to the systematic uncertainty are listed in Table 1. The systematic uncertainties due to the tracking efficiencies and PID efficiencies are $^{+15}_{-18}(\pm 15)$% for $p_T < 2$ GeV/c ($2 < p_T < 6$ GeV/c). These reach $\approx^{+20}_{-40}$% at 8 GeV/c due to the uncertainty of the hadron contamination subtraction, which is $\approx^{+8}_{-30}$% at 8 GeV/c. Additional contributions to the total systematic uncertainty include the d_0 selection, evaluated by repeating the full analysis with modified selection criteria, and the subtraction of light flavor hadron decay background and charm hadron decay background, which were obtained by propagating the statistical and systematic uncertainties of the light flavor and charm hadron measurements used as analysis input. The light hadron decay background systematic uncertainty includes the uncertainty of the m_T-scaling, which is conservatively taken to be 30%. All systematic uncertainties were added in quadrature to obtain the total systematic uncertainty.

3.2. Azimuthal electron–hadron correlation technique

This analysis is based on the shape of the distribution of the difference in azimuth ($\Delta\varphi$) between electrons and hadrons, and in

Table 1
Contributions to the systematic uncertainty of the measurement of electrons from beauty hadron decays with the impact parameter method, for the ranges $1 < p_T < 2$ GeV/c (centre column) and $2 < p_T < 8$ GeV/c (right column). The total systematic uncertainty is calculated as the quadrature sum of all contributions.

Uncertainty source	Systematic uncertainty (%) $1 < p_T < 2$ GeV/c	$2 < p_T < 8$ GeV/c
Track matching	±2	±2
ITS number of hits	±10	±10
Number of TPC clusters for tracking	+1, −10	±1
Number of TPC clusters for PID	±3	±3
TOF PID	±3	n.a.
TPC PID	±10	±10
Track η and charge dependence	±2	±2
Minimum d_0 requirement	+15, −25	±15
Light hadron decay background	≈15	<3
Charm hadron decay background	+40, −60	<10

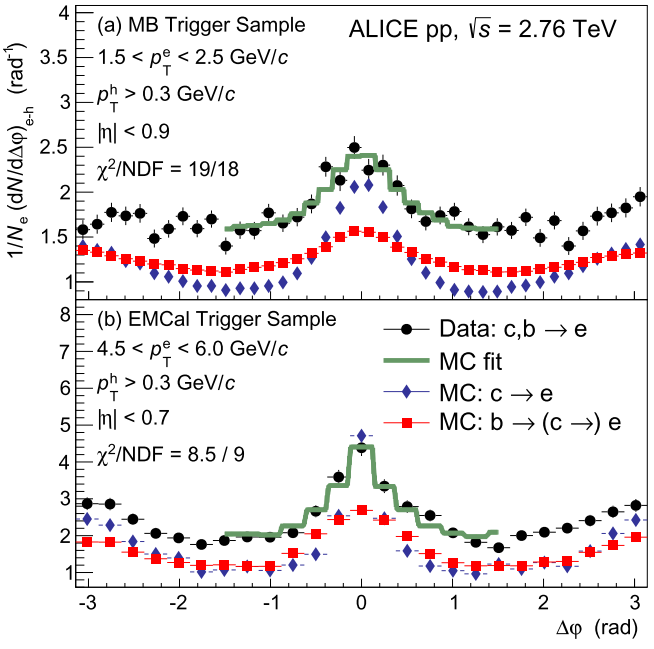

Fig. 3. (Colour online.) The azimuthal correlation between heavy-flavour decay electrons and charged hadrons, scaled by the number of electrons is shown for (a) the MB events in the p_T^e range 1.5 to 2.5 GeV/c and (b) the EMCal events in the p_T^e range 4.5 to 6.0 GeV/c. The diamonds represent the MC distribution for electrons from charm hadron decays, squares are the MC distribution for electrons from beauty hadron decays. The line is the MC fit (Eq. (2)) to the data points (circles).

particular of the peak at $\Delta\varphi$ around zero (near-side). Due to the different decay kinematics of charm and beauty hadrons, the width of the near-side peak is larger for beauty than for charm hadron decays. This method has been previously used by the STAR experiment [29]. A similar method based on the invariant mass of like charge sign electron–kaon pairs [30] was used by the PHENIX experiment to extract a relative beauty contribution to the measured heavy-flavour electron production cross section.

The analysis was performed using the MB and EMCal trigger data sets. Electrons were selected in the range $1 < p_T < 10$ GeV/c. For the MB analysis the selected electrons reached out to a transverse momentum of 6 GeV/c, while the analysis using EMCal triggered events selects electrons in the range $2.5 < p_T < 10$ GeV/c.

The electron sample ($N_{e_{incl}}$) contains electrons from heavy-flavour hadron decays and the aforementioned background sources, listed in Section 3.1. Di-electron pairs from photon conversions and π^0 Dalitz decays dominate at low p_T and were identified by pairing electrons with oppositely charged partner tracks and calculating the invariant mass ($M_{e^+e^-}$) of each e^+e^- pair. The distribution for the background electrons is peaked at low $M_{e^+e^-}$, while no correlation signal is present in the low $M_{e^+e^-}$ region for the electrons from heavy-flavour decays. These unlike charge-sign (ULS) pairs contain true conversion and Dalitz decay electrons, along with a small fraction of heavy-flavour electrons that were wrongly paired with a background electron. The latter can be identified by calculating the invariant mass of like charge-sign (LS) pairs. Using a MC simulation with GEANT3, where pp collisions are generated using PYTHIA 6 (Perugia-0 tune) and by comparing the ULS and LS invariant mass distribution the selection criteria on $M_{e^+e^-}$, identical for the LS and ULS pairs, were determined. Electrons with $M_{e^+e^-} < 50(100)$ MeV/c^2 for the EMCal(MB) analysis were identified as background. The background finding efficiency (ϵ) ranges from ∼20% at low p_T to ∼66% for p_T above 4 GeV/c.

The number of heavy-flavour hadron decay electrons can be expressed as

$$N_{e_{HF}} = N_{e_{incl}} - \frac{1}{\epsilon}(N_{e_{ULS}} - N_{e_{LS}}), \tag{1}$$

where $N_{e_{ULS}}$ ($N_{e_{LS}}$) are the number of electrons which formed a ULS(LS) pair with a $M_{e^+e^-}$ satisfying the previously mentioned selection criteria. Each electron contribution from Eq. (1) is taken, along with the charged hadrons in the event and the heavy-flavour decay electron–hadron azimuthal correlation distribution, $\frac{1}{N_e}(\frac{dN}{d\Delta\varphi})_{e_{HF}-h}$, was constructed.

To determine the fraction of electrons from beauty hadron decays the measured azimuthal e–h correlation distribution was fit with the function

$$\frac{1}{N_{e_{HF}}}\left(\frac{dN}{d\Delta\varphi}\right)_{e_{HF}-h} = C + r_b \frac{1}{N_{e_b}}\left(\frac{dN}{d\Delta\varphi}\right)_{e_b-h} + (1-r_b)\frac{1}{N_{e_c}}\left(\frac{dN}{d\Delta\varphi}\right)_{e_c-h}, \tag{2}$$

where r_b, a free parameter of the fit, is the fraction of electrons from beauty to the total number of electrons from all heavy-flavour decays, $\Delta\varphi$ is the azimuthal angle between the electron and the charged hadron. The distributions of the azimuthal correlations $(\frac{dN}{d\Delta\varphi})_{e_{b(c)}-h}$ for electrons from beauty (charm) hadron decays were taken from the previously mentioned MC simulation, and the constant C accounts for the uncorrelated background. Fig. 3 shows the measured azimuthal correlation, scaled by the number of electrons, along with the MC fit templates and the full fit for both (a) the MB and (b) the EMCal trigger analyses, in the p_T range of 1.5–2.5 GeV/c and 4.5–6 GeV/c, respectively. For each p_T bin the measured distribution was fit on the near-side, over the range $|\Delta\varphi| < 1.5$ rad. From the fit, the relative beauty fraction (r_b) is extracted as a function of p_T. The values of r_b obtained from the MB and EMCal triggered samples were found to agree within the

Table 2
Contributions to the systematic uncertainty of the fraction of electrons from beauty to the total number of electrons from heavy-flavour decays measured using the e–h azimuthal correlation technique, for the MB trigger (centre column) and EMCal trigger (right column) analyses. The total systematic uncertainty is calculated as the quadrature sum of all contributions.

Uncertainty source	Systematic uncertainty (%) MB	EMCal
Number of TPC clusters for tracking	±8	5
TPC PID	±5 (+5, −20) for $p_T < (>)3.5$ GeV/c	±5 (±10) for $p_T < (>)3.5$ GeV/c
TOF PID	±5	n.a.
EMCal PID	n.a.	±10 (±5) for $p_T < (>)3.5$ GeV/c
e^+e^- invariant mass	negligible	±10 (±5) for $p_T < (>)3.5$ GeV/c
Associated electron PID	±1	±1 (±5) for $p_T < (>)4.5$ GeV/c
Associated hadron momentum	±8	±10 (±5) for $p_T < (>)3.5$ GeV/c
Fit range	negligible	negligible (±5) for $p_T < (> 6)$ GeV/c
Light hadron decay background	±1	±25 (±5) for $p_T < (>)3.5$ GeV/c

systematic and statistical uncertainties in the overlapping p_T intervals. Hence, in the common p_T range, the final results for the relative beauty contribution to heavy-flavour decay electrons was obtained as the weighted average of the results from the MB and EMCal samples.

The main sources of systematic uncertainty include the electron identification selection criteria and the background finding efficiency. As previously explained, the background electrons were identified using invariant mass $M_{e^+e^-}$. The selected mass requirement, as a source of systematic uncertainty was found to be negligible for the MB analysis and reached a maximum of 10% for $p_T < 3.5$ GeV for the EMCal analysis. The efficiency of the invariant mass method was calculated using a MC sample. For the EMCal analysis a MC simulation enhanced with π^0 and η mesons, flat in p_T, was used in order to increase statistics of background electrons at high p_T, as the MB MC sample did not provide enough statistics. The bias from the enhancement is corrected by reweighting to obtain the correct p_T-distribution of the π^0 (see Section 3.1). Overall, the systematic uncertainties range from 9 to 21% for the MB analysis and from 12 to 33% in the case of the EMCal analysis, depending on the transverse momentum. The final systematic uncertainties were obtained by combining these two measurements, yielding 17% for the lower momentum region ($p_T < 3.5$ GeV/c) and $^{+16}_{-25}$% for the higher momentum region ($3.5 < p_T < 10$ GeV/c). All systematic uncertainties are listed in Table 2.

For the MB analysis the hadron contamination to the electron sample was estimated using a simultaneous fit of the electron and the different hadron components of the TPC dE/dx distribution in momentum ranges, while for the EMCal analysis the contamination was estimated using a fit to the E/p distribution in momentum slices. The contamination was found to be negligible for $p_T < 4(6)$ GeV/c for the MB(EMCal) analysis. For the highest p_T of the MB analysis the contamination was 5% and reached 20% for the highest p_T of the EMCal analysis. No subtraction of this contamination was performed. Instead it is taken into account in the PID systematic uncertainties. In addition, a mixed event technique was used to cross-check that detector acceptance effects are well reproduced in the MC sample. For the mixed event $\Delta\varphi$ correlation distribution, electrons from EMCal trigger events and hadrons from the MB sample were selected. Hadrons were selected only from MB events to remove the bias from EMCal trigger sample in the correlation distribution from mixed event. The mixed event correlation distribution was found to be flat over the entire $\Delta\varphi$ range, implying that detector effects do not bias the correlation distribution. Hence a mixed event correction was not applied to the resulting $\Delta\varphi$ distribution.

4. Results

The relative beauty contribution to heavy-flavour decay electrons obtained from the impact parameter analysis, along with

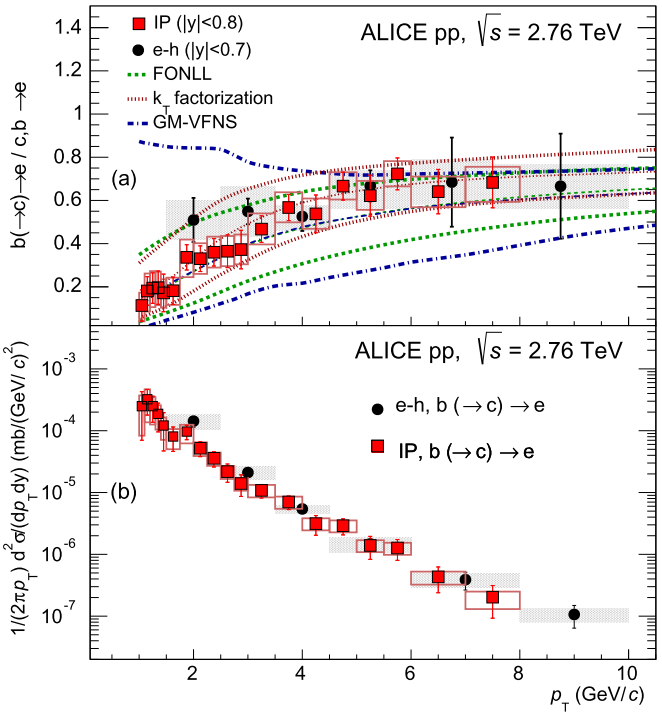

Fig. 4. (Colour online.) (a) Relative beauty contribution to the heavy-flavour electron yield; measured from the azimuthal correlations between heavy-flavour decay electrons and charged hadrons (black circles) compared to that from the method based on the track impact parameter (red squares). The green dashed, red dotted, and blue dot-dashed lines represent the FONLL [1], k_T-factorization [3], and GM-VFNS [16] predictions, respectively. (b) The p_T-differential inclusive production cross section of electrons from beauty hadron decays obtained using the impact parameter method (red squares) and the e–h correlation (black circles) method. For both panels, the error bars (boxes) represent the statistical (systematic) uncertainties. The notation b(→ c) → e is used to indicate that the relative beauty contribution includes those electrons which originate directly from beauty hadron decays and those which originate from charm hadron decays, where the charm hadron is the decay product of a beauty hadron.

that extracted from the azimuthal correlation method, is shown as a function of p_T in Fig. 4(a). For the impact parameter analysis the beauty contribution to the heavy-flavour electron spectrum was measured, while the charm contribution was calculated from the charm hadron spectra measured by ALICE as described in Section 3.1. Within the statistical and systematic uncertainties the resulting fractions are in agreement with each other and show that the beauty contribution to the total heavy-flavour spectrum is comparable to the contribution from charm for $p_T > 4$ GeV/c.

The measurements are compared to the central, upper, and lower predictions of three sets of pQCD calculations [1,16,3], represented by the various lines. The central values of the fraction of electrons from beauty hadron decays were calculated using the

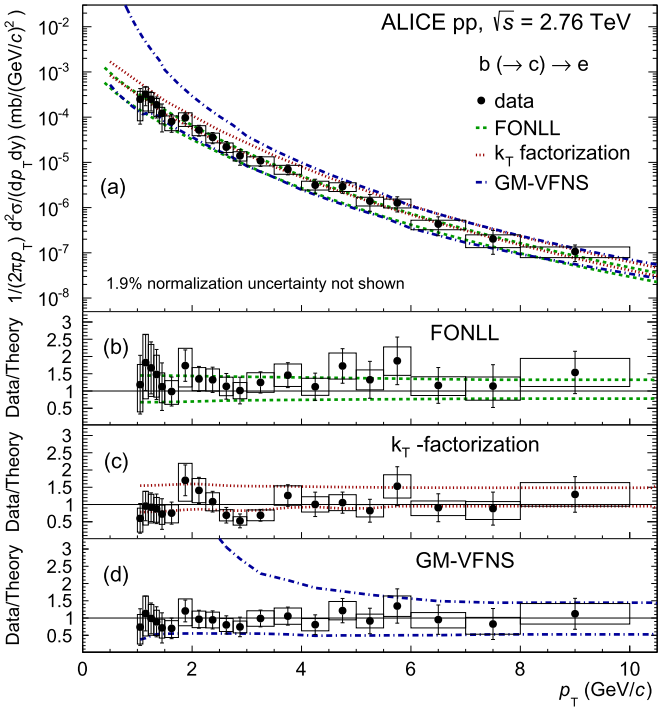

Fig. 5. (Colour online.) (a) p_{T}-differential inclusive production cross section of electrons from beauty hadron decays. The green dashed, red dotted, and blue dot-dashed lines represent the FONLL [1], k_{T}-factorization [3], and GM-VFNS [16] uncertainty range, respectively. (b)–(d) Ratios of the data and the central prediction of pQCD calculations for electrons from beauty hadron decays. For all panels, the error bars (boxes) represent the statistical (systematic) uncertainties.

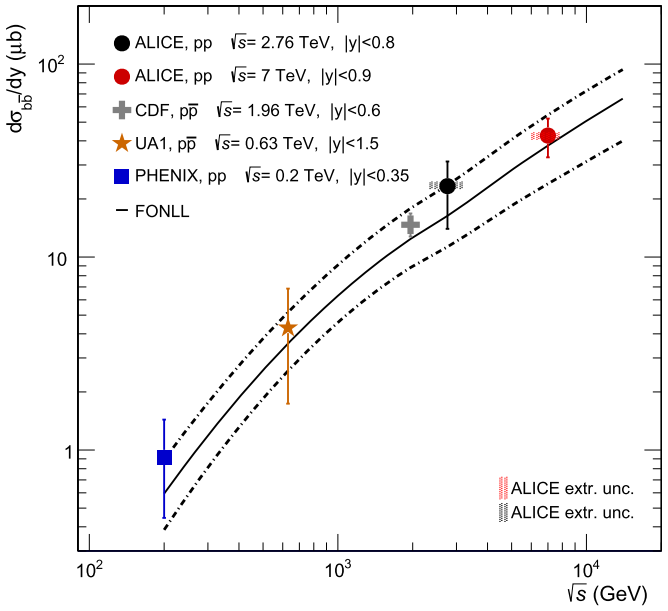

Fig. 6. (Colour online.) Inclusive beauty production cross section per rapidity unit measured at mid-rapidity as a function of centre of mass energy in pp collisions (PHENIX [30] and ALICE [22] results) and p$\bar{\mathrm{p}}$ collisions (UA1 [31] and CDF [32] results) along with the comparison to FONLL calculations. Error bars represent the statistical and systematic uncertainties added in quadrature. The FONLL calculation was performed for the five experimental rapidity ranges and centre of mass energies shown in the figure, and these points are drawn as a curve.

central values of the beauty and charm to electron cross sections. The upper (lower) predictions were obtained by calculating the beauty fraction using the upper (lower) uncertainty limit of the beauty to electron cross section and the lower (upper) limit of the charm to electron cross section. The upper and lower lines demonstrate the uncertainty range of the calculations, which originate from the variation of the perturbative scales and the heavy quark masses as described in [1–3]. Each prediction describes the relative beauty contribution fraction over the whole p_{T} range.

The p_{T}-differential production cross section of electrons from beauty hadron decays measured using the impact parameter analysis is shown in Fig. 4(b) and it is compared to the spectrum obtained using the beauty fraction from the e–h correlation analysis and the measured heavy-flavour decay electron cross section from [13]. This alternative approach agrees with the result obtained using the impact parameter technique. As the resulting spectrum obtained using the impact parameter based analysis ($|y| < 0.8$) yielded finer p_{T} intervals and smaller uncertainties this result for $p_{\mathrm{T}} < 8$ GeV/c is used with the higher p_{T} slice of the e–h correlation analysis ($|y| < 0.7$) to obtain the total beauty production cross section.

The measured p_{T}-differential cross section, obtained using the impact parameter analysis for $p_{\mathrm{T}} < 8$ GeV/c and including the highest p_{T} point from the correlation analysis, in the p_{T} range 1–10 GeV/c is shown in Fig. 5(a) along with a comparison to the upper and lower uncertainty limits of the aforementioned pQCD calculations. Fig. 5(b)–(d) shows the ratio of the data to the central theoretical predictions. The data and predictions are consistent within the experimental and theoretical uncertainties. Due to the uncertainty of the measured luminosity all measured cross sections have an additional normalization uncertainty of 1.9% [17].

The visible cross section of electrons from beauty hadron decays at mid-rapidity ($|y| < 0.8$) was obtained by integrating the p_{T}-differential cross section in the measured p_{T} range ($1 < p_{\mathrm{T}} < 10$ GeV/c), obtaining $\sigma_{\mathrm{b}\to\mathrm{e}} = 3.47 \pm 0.40(\mathrm{stat})^{+1.12}_{-1.33}(\mathrm{sys}) \pm 0.07(\mathrm{norm})$ μb. The visible cross section is then scaled by the ratio of the total cross section of electrons originating from beauty hadron decays from FONLL in the full p_{T} range to the FONLL cross section integrated in the measured p_{T} range. The central value of the extrapolation factor was computed using the FONLL prediction with the central values of the quark mass and perturbative scale. The uncertainties were obtained by varying the quark mass and perturbative scale and recalculating the ratio, which is given separately in the results as extrapolation uncertainty. For the extrapolation the beauty hadron to electron branching ratio of $\mathrm{BR}_{\mathrm{H_b}\to\mathrm{e}} + \mathrm{BR}_{\mathrm{H_b}\to\mathrm{H_c}\to\mathrm{e}} = 0.205 \pm 0.007$ [33] is used.

The beauty production cross section at mid-rapidity, per unit rapidity, $\frac{\mathrm{d}\sigma_{\mathrm{b\bar{b}}}}{\mathrm{dy}} = 23.28 \pm 2.70(\mathrm{stat})^{+8.92}_{-8.70}(\mathrm{sys})^{+0.49}_{-0.65}(\mathrm{extr}) \pm 0.44(\mathrm{norm})$ μb, is shown in Fig. 6 as a function of centre of mass energy for experimental measurements [30,32,31], including the result obtained by ALICE at 7 TeV [22]. The total beauty production cross section was obtained by extrapolating to the full y range and is found to be $\sigma_{\mathrm{b\bar{b}}} = 130 \pm 15.1(\mathrm{stat})^{+42.1}_{-49.8}(\mathrm{sys})^{+3.4}_{-3.1}(\mathrm{extr}) \pm 2.5(\mathrm{norm}) \pm 4.4(\mathrm{BR})$ μb. The corresponding prediction of FONLL is $\sigma_{\mathrm{b\bar{b}}} = 95.5^{+139}_{-66.5}$ μb.

5. Summary

The inclusive invariant production cross section of electrons from semi-leptonic decays of beauty hadrons is reported at mid-rapidity ($|y| < 0.8$) in the transverse momentum range $1 < p_{\mathrm{T}} < 10$ GeV/c, in pp collisions at $\sqrt{s} = 2.76$ TeV. The primary measurement utilized a selection of tracks based on their impact parameter to identify displaced electrons from beauty hadron decays. An alternative method, which utilized the measured electron–hadron azimuthal correlations, was found to be in agreement with the results from the impact parameter method. The results are compared to pQCD calculations and agreement between data and theory

was found. The integrated visible cross section is $\sigma_{b\to e} = 3.47 \pm 0.40(\text{stat})^{+1.12}_{-1.33}(\text{sys}) \pm 0.07(\text{norm})$ μb. Extrapolation to full phase space using FONLL yields the total $b\bar{b}$ production cross section, $\sigma_{b\bar{b}} = 130 \pm 15.1(\text{stat})^{+42.1}_{-49.8}(\text{sys})^{+3.4}_{-3.1}(\text{extr}) \pm 2.5(\text{norm}) \pm 4.4(\text{BR})$ μb. These results provide a crucial reference for the study of beauty quark production in Pb–Pb collisions at the LHC.

Acknowledgements

The ALICE Collaboration would like to thank all its engineers and technicians for their invaluable contributions to the construction of the experiment and the CERN accelerator teams for the outstanding performance of the LHC complex. The ALICE Collaboration gratefully acknowledges the resources and support provided by all Grid centres and the Worldwide LHC Computing Grid (WLCG) Collaboration. The ALICE Collaboration acknowledges the following funding agencies for their support in building and running the ALICE detector: State Committee of Science, World Federation of Scientists (WFS) and Swiss Fonds Kidagan, Armenia, Conselho Nacional de Desenvolvimento Científico e Tecnológico (CNPq), Financiadora de Estudos e Projetos (FINEP), Fundação de Amparo à Pesquisa do Estado de São Paulo (FAPESP); National Natural Science Foundation of China (NSFC), the Chinese Ministry of Education (CMOE) and the Ministry of Science and Technology of China (MSTC); Ministry of Education and Youth of the Czech Republic; Danish Natural Science Research Council, the Carlsberg Foundation and the Danish National Research Foundation; The European Research Council under the European Community's Seventh Framework Programme; Helsinki Institute of Physics and the Academy of Finland; French CNRS-IN2P3, the 'Region Pays de Loire', 'Region Alsace', 'Region Auvergne' and CEA, France; German BMBF and the Helmholtz Association; General Secretariat for Research and Technology, Ministry of Development, Greece; Hungarian OTKA and National Office for Research and Technology (NKTH); Department of Atomic Energy and Department of Science and Technology of the Government of India; Istituto Nazionale di Fisica Nucleare (INFN) and Centro Fermi – Museo Storico della Fisica e Centro Studi e Ricerche "Enrico Fermi", Italy; MEXT Grant-in-Aid for Specially Promoted Research, Japan; Joint Institute for Nuclear Research, Dubna; National Research Foundation of Korea (NRF); CONACYT, DGAPA, México, ALFA-EC and the EPLANET Program (European Particle Physics Latin American Network) Stichting voor Fundamenteel Onderzoek der Materie (FOM) and the Nederlandse Organisatie voor Wetenschappelijk Onderzoek (NWO), Netherlands; Research Council of Norway (NFR); Polish Ministry of Science and Higher Education; National Science Centre, Poland; Ministry of National Education/Institute for Atomic Physics and CNCS-UEFISCDI – Romania; Ministry of Education and Science of Russian Federation, Russian Academy of Sciences, Russian Federal Agency of Atomic Energy, Russian Federal Agency for Science and Innovations and The Russian Foundation for Basic Research; Ministry of Education of Slovakia; Department of Science and Technology, South Africa; CIEMAT, EELA, Ministerio de Economía y Competitividad (MINECO) of Spain, Xunta de Galicia (Consellería de Educación), CEADEN, Cubaenergía, Cuba, and IAEA (International Atomic Energy Agency); Swedish Research Council (VR) and Knut & Alice Wallenberg Foundation (KAW); Ukraine Ministry of Education and Science; United Kingdom Science and Technology Facilities Council (STFC); The United States Department of Energy, the United States National Science Foundation, the State of Texas, and the State of Ohio.

References

[1] M. Cacciari, S. Frixione, N. Houdeau, M.L. Mangano, P. Nason, et al., Theoretical predictions for charm and bottom production at the LHC, J. High Energy Phys. 1210 (2012) 137.
[2] B. Kniehl, G. Kramer, I. Schienbein, H. Spiesberger, Inclusive charmed-meson production at the CERN LHC, Eur. Phys. J. C 72 (2012) 2082.
[3] R. Maciula, A. Szczurek, Open charm production at the LHC – k_t-factorization approach, Phys. Rev. D 87 (2013) 094022.
[4] I. Arsene, et al., BRAHMS Collaboration, Quark gluon plasma and color glass condensate at RHIC? The perspective from the BRAHMS experiment, Nucl. Phys. A 757 (2005) 1.
[5] K. Adcox, et al., PHENIX Collaboration, Formation of dense partonic matter in relativistic nucleus–nucleus collisions at RHIC: experimental evaluation by the PHENIX Collaboration, Nucl. Phys. A 757 (2005) 184.
[6] B. Back, M. Baker, M. Ballintijn, D. Barton, B. Becker, et al., The PHOBOS perspective on discoveries at RHIC, Nucl. Phys. A 757 (2005) 28.
[7] J. Adams, et al., STAR Collaboration, Experimental and theoretical challenges in the search for the quark gluon plasma: the STAR Collaboration's critical assessment of the evidence from RHIC collisions, Nucl. Phys. A 757 (2005) 102.
[8] B. Abelev, et al., ALICE Collaboration, Suppression of high transverse momentum D mesons in central Pb–Pb collisions at $\sqrt{s_{NN}} = 2.76$ TeV, J. High Energy Phys. 1209 (2012) 112.
[9] B. Abelev, et al., ALICE Collaboration, D meson elliptic flow in non-central Pb–Pb collisions at $\sqrt{s_{NN}} = 2.76$ TeV, Phys. Rev. Lett. 111 (2013) 102301.
[10] S. Chatrchyan, et al., CMS Collaboration, Evidence of b-jet quenching in PbPb collisions at $\sqrt{s_{NN}} = 2.76$ TeV, arXiv:1312.4198 [nucl-ex], 2013.
[11] S. Chatrchyan, et al., CMS Collaboration, Suppression of non-prompt J/ψ, prompt J/ψ, and Υ(1S) in PbPb collisions at $\sqrt{s_{NN}} = 2.76$ TeV, J. High Energy Phys. 1205 (2012) 063.
[12] B. Abelev, et al., ALICE Collaboration, Measurement of charm production at central rapidity in proton–proton collisions at $\sqrt{s} = 2.76$ TeV, J. High Energy Phys. 1207 (2012) 191.
[13] B. Abelev, et al., ALICE Collaboration, Measurement of electrons from semileptonic heavy-flavor hadron decays in pp collisions at $\sqrt{s} = 2.76$ TeV, arXiv:1405.4117 [nucl-ex], 2014.
[14] B. Abelev, et al., ALICE Collaboration, Production of muons from heavy flavor decays at forward rapidity in pp and Pb–Pb collisions at $\sqrt{s_{NN}} = 2.76$ TeV, Phys. Rev. Lett. 109 (2012) 112301.
[15] B. Abelev, et al., ALICE Collaboration, Inclusive J/ψ production in pp collisions at $\sqrt{s} = 2.76$ TeV, Phys. Lett. B 718 (2012) 295.
[16] P. Bolzoni, G. Kramer, Inclusive lepton production from heavy-hadron decay in pp collisions at the LHC, Nucl. Phys. B 872 (2013) 253.
[17] B. Abelev, et al., ALICE Collaboration, Measurement of inelastic, single- and double-diffraction cross sections in proton–proton collisions at the LHC with ALICE, Eur. Phys. J. C 73 (2013) 2456.
[18] B. Abelev, et al., ALICE Collaboration, Measurement of the inclusive differential jet cross section in pp collisions at $\sqrt{s} = 2.76$ TeV, Phys. Lett. B 722 (2013) 262.
[19] J. Kral, T. Awes, H. Muller, J. Rak, J. Schambach, L0 trigger for the EMCal detector of the ALICE experiment, Nucl. Instrum. Methods A 693 (2012) 261.
[20] J. Alme, et al., The ALICE TPC, a large 3-dimensional tracking device with fast readout for ultra-high multiplicity events, Nucl. Instrum. Methods A 622 (2010) 316.
[21] K. Aamodt, et al., ALICE Collaboration, Alignment of the ALICE Inner Tracking System with cosmic-ray tracks, J. Instrum. 5 (2010) P03003.
[22] B. Abelev, et al., ALICE Collaboration, Measurement of electrons from beauty hadron decays in pp collisions at $\sqrt{s} = 7$ TeV, Phys. Lett. B 721 (2013) 13.
[23] R. Brun, et al., CERN Program Library Long Write-up, W5013, 1994.
[24] P.Z. Skands, The Perugia Tunes, arXiv:0905.3418 [hep-ph], 2009.
[25] B. Abelev, et al., ALICE Collaboration, Neutral pion production at midrapidity in pp and PbPb collisions at $\sqrt{s_{NN}} = 2.76$ TeV, arXiv:1405.3794 [nucl-ex], 2014.
[26] K. Aamodt, et al., ALICE Collaboration, Measurement of charm production at central rapidity in proton–proton collisions at $\sqrt{s} = 7$ TeV, J. High Energy Phys. 01 (2012) 128.
[27] R. Averbeck, N. Bastid, Z.C. del Valle, P. Crochet, A. Dainese, et al., Reference heavy flavour cross sections in pp collisions at $\sqrt{s} = 2.76$ TeV, using a pQCD-driven $\sqrt{s}$-scaling of ALICE measurements at $\sqrt{s} = 7$ TeV, arXiv:1107.3243 [hep-ph], 2011.
[28] S. Chekanov, et al., ZEUS Collaboration, Measurement of charm fragmentation ratios and fractions in photoproduction at HERA, Eur. Phys. J. C 44 (2005) 351.
[29] M. Aggarwal, et al., STAR Collaboration, Measurement of the bottom contribution to non-photonic electron production in pp collisions at $\sqrt{s} = 200$ GeV, Phys. Rev. Lett. 105 (2010) 202301.
[30] A. Adare, et al., PHENIX Collaboration, Measurement of bottom versus charm as a function of transverse momentum with electron–hadron correlations in pp collisions at $\sqrt{s} = 200$ GeV, Phys. Rev. Lett. 103 (2009) 082002.
[31] C. Albajar, et al., UA1 Collaboration, Beauty production at the CERN p anti-p collider, Phys. Lett. B 256 (1991) 121.

[32] D. Acosta, et al., CDF Collaboration, Measurement of the J/ψ meson and b-hadron production cross sections in $p\bar{p}$ collisions at $\sqrt{s} = 1960$ GeV, Phys. Rev. D 71 (2005) 032001.

[33] J. Beringer, et al., Particle Data Group, The review of particle physics, Phys. Rev. D 86 (2012) 010001.

ALICE Collaboration

B. Abelev [bs], J. Adam [ak], D. Adamová [ca], M.M. Aggarwal [ce], G. Aglieri Rinella [ah], M. Agnello [dc,cl], A. Agostinelli [z], N. Agrawal [ar], Z. Ahammed [dv], N. Ahmad [r], I. Ahmed [o], S.U. Ahn [bl], S.A. Ahn [bl], I. Aimo [dc,cl], S. Aiola [ea], M. Ajaz [o], A. Akindinov [bb], S.N. Alam [dv], D. Aleksandrov [cr], B. Alessandro [dc], D. Alexandre [ct], A. Alici [l,cw], A. Alkin [c], J. Alme [ai], T. Alt [am], S. Altinpinar [q], I. Altsybeev [du], C. Alves Garcia Prado [dk], C. Andrei [bv], A. Andronic [co], V. Anguelov [ck], J. Anielski [ax], T. Antičić [cp], F. Antinori [cz], P. Antonioli [cw], L. Aphecetche [de], H. Appelshäuser [aw], S. Arcelli [z], N. Armesto [p], R. Arnaldi [dc], T. Aronsson [ea], I.C. Arsene [co,u], M. Arslandok [aw], A. Augustinus [ah], R. Averbeck [co], T.C. Awes [cb], M.D. Azmi [r,cg], M. Bach [am], A. Badalà [cy], Y.W. Baek [an,bn], S. Bagnasco [dc], R. Bailhache [aw], R. Bala [ch], A. Baldisseri [n], F. Baltasar Dos Santos Pedrosa [ah], R.C. Baral [be], R. Barbera [aa], F. Barile [ae], G.G. Barnaföldi [dz], L.S. Barnby [ct], V. Barret [bn], J. Bartke [dh], M. Basile [z], N. Bastid [bn], S. Basu [dv], B. Bathen [ax], G. Batigne [de], A. Batista Camejo [bn], B. Batyunya [bj], P.C. Batzing [u], C. Baumann [aw], I.G. Bearden [bx], H. Beck [aw], C. Bedda [cl], N.K. Behera [ar], I. Belikov [ay], F. Bellini [z], R. Bellwied [dm], E. Belmont-Moreno [bh], R. Belmont III [dy], V. Belyaev [bt], G. Bencedi [dz], S. Beole [y], I. Berceanu [bv], A. Bercuci [bv], Y. Berdnikov [cc,1], D. Berenyi [dz], M.E. Berger [cj], R.A. Bertens [ba], D. Berzano [y], L. Betev [ah], A. Bhasin [ch], I.R. Bhat [ch], A.K. Bhati [ce], B. Bhattacharjee [ao], J. Bhom [dr], L. Bianchi [y], N. Bianchi [bp], C. Bianchin [ba], J. Bielčík [ak], J. Bielčíková [ca], A. Bilandzic [bx], S. Bjelogrlic [ba], F. Blanco [j], D. Blau [cr], C. Blume [aw], F. Bock [br,ck], A. Bogdanov [bt], H. Bøggild [bx], M. Bogolyubsky [dd], F.V. Böhmer [cj], L. Boldizsár [dz], M. Bombara [al], J. Book [aw], H. Borel [n], A. Borissov [dy,cn], F. Bossú [bi], M. Botje [by], E. Botta [y], S. Böttger [av], P. Braun-Munzinger [co], M. Bregant [dk], T. Breitner [av], T.A. Broker [aw], T.A. Browning [cm], M. Broz [ak], E. Bruna [dc], G.E. Bruno [ae], D. Budnikov [cq], H. Buesching [aw], S. Bufalino [dc], P. Buncic [ah], O. Busch [ck], Z. Buthelezi [bi], D. Caffarri [ah,ab], X. Cai [g], H. Caines [ea], L. Calero Diaz [bp], A. Caliva [ba], E. Calvo Villar [cu], P. Camerini [x], F. Carena [ah], W. Carena [ah], J. Castillo Castellanos [n], E.A.R. Casula [w], V. Catanescu [bv], C. Cavicchioli [ah], C. Ceballos Sanchez [i], J. Cepila [ak], P. Cerello [dc], B. Chang [dn], S. Chapeland [ah], J.L. Charvet [n], S. Chattopadhyay [dv], S. Chattopadhyay [cs], V. Chelnokov [c], M. Cherney [cd], C. Cheshkov [dt], B. Cheynis [dt], V. Chibante Barroso [ah], D.D. Chinellato [dl,dm], P. Chochula [ah], M. Chojnacki [bx], S. Choudhury [dv], P. Christakoglou [by], C.H. Christensen [bx], P. Christiansen [af], T. Chujo [dr], S.U. Chung [cn], C. Cicalo [cx], L. Cifarelli [z,l], F. Cindolo [cw], J. Cleymans [cg], F. Colamaria [ae], D. Colella [ae], A. Collu [w], M. Colocci [z], G. Conesa Balbastre [bo], Z. Conesa del Valle [au], M.E. Connors [ea], J.G. Contreras [k,ak], T.M. Cormier [cb,dy], Y. Corrales Morales [y], P. Cortese [ad], I. Cortés Maldonado [b], M.R. Cosentino [dk], F. Costa [ah], P. Crochet [bn], R. Cruz Albino [k], E. Cuautle [bg], L. Cunqueiro [bp,ah], A. Dainese [cz], R. Dang [g], A. Danu [bf], D. Das [cs], I. Das [au], K. Das [cs], S. Das [d], A. Dash [dl], S. Dash [ar], S. De [dv], H. Delagrange [de,2], A. Deloff [bu], E. Dénes [dz], G. D'Erasmo [ae], A. De Caro [ac,l], G. de Cataldo [cv], J. de Cuveland [am], A. De Falco [w], D. De Gruttola [ac,l], N. De Marco [dc], S. De Pasquale [ac], R. de Rooij [ba], M.A. Diaz Corchero [j], T. Dietel [ax,cg], P. Dillenseger [aw], R. Divià [ah], D. Di Bari [ae], S. Di Liberto [da], A. Di Mauro [ah], P. Di Nezza [bp], Ø. Djuvsland [q], A. Dobrin [ba], T. Dobrowolski [bu], D. Domenicis Gimenez [dk], B. Dönigus [aw], O. Dordic [u], S. Dørheim [cj], A.K. Dubey [dv], A. Dubla [ba], L. Ducroux [dt], P. Dupieux [bn], A.K. Dutta Majumdar [cs], T.E. Hilden [ap], R.J. Ehlers [ea], D. Elia [cv], H. Engel [av], B. Erazmus [ah,de], H.A. Erdal [ai], D. Eschweiler [am], B. Espagnon [au], M. Esposito [ah], M. Estienne [de], S. Esumi [dr], D. Evans [ct], S. Evdokimov [dd], D. Fabris [cz], J. Faivre [bo], D. Falchieri [z], A. Fantoni [bp], M. Fasel [ck], D. Fehlker [q], L. Feldkamp [ax], D. Felea [bf], A. Feliciello [dc], G. Feofilov [du], J. Ferencei [ca], A. Fernández Téllez [b], E.G. Ferreiro [p], A. Ferretti [y], A. Festanti [ab], J. Figiel [dh], M.A.S. Figueredo [do], S. Filchagin [cq], D. Finogeev [az], F.M. Fionda [ae], E.M. Fiore [ae], E. Floratos [cf], M. Floris [ah], S. Foertsch [bi], P. Foka [co], S. Fokin [cr], E. Fragiacomo [db], A. Francescon [ah,ab], U. Frankenfeld [co], U. Fuchs [ah], C. Furget [bo], M. Fusco Girard [ac], J.J. Gaardhøje [bx], M. Gagliardi [y], A.M. Gago [cu], M. Gallio [y], D.R. Gangadharan [s,br], P. Ganoti [cb,cf], C. Gao [g], C. Garabatos [co], E. Garcia-Solis [m], C. Gargiulo [ah], I. Garishvili [bs], J. Gerhard [am], M. Germain [de], A. Gheata [ah], M. Gheata [ah,bf], B. Ghidini [ae], P. Ghosh [dv], S.K. Ghosh [d], P. Gianotti [bp], P. Giubellino [ah], E. Gladysz-Dziadus [dh], P. Glässel [ck], A. Gomez Ramirez [av], P. González-Zamora [j], S. Gorbunov [am], L. Görlich [dh], S. Gotovac [dg],

L.K. Graczykowski [dx], A. Grelli [ba], A. Grigoras [ah], C. Grigoras [ah], V. Grigoriev [bt], A. Grigoryan [a], S. Grigoryan [bj], B. Grinyov [c], N. Grion [db], J.F. Grosse-Oetringhaus [ah], J.-Y. Grossiord [dt], R. Grosso [ah], F. Guber [az], R. Guernane [bo], B. Guerzoni [z], M. Guilbaud [dt], K. Gulbrandsen [bx], H. Gulkanyan [a], M. Gumbo [cg], T. Gunji [dq], A. Gupta [ch], R. Gupta [ch], K.H. Khan [o], R. Haake [ax], Ø. Haaland [q], C. Hadjidakis [au], M. Haiduc [bf], H. Hamagaki [dq], G. Hamar [dz], L.D. Hanratty [ct], A. Hansen [bx], J.W. Harris [ea], H. Hartmann [am], A. Harton [m], D. Hatzifotiadou [cw], S. Hayashi [dq], S.T. Heckel [aw], M. Heide [ax], H. Helstrup [ai], A. Herghelegiu [bv], G. Herrera Corral [k], B.A. Hess [ag], K.F. Hetland [ai], B. Hippolyte [ay], J. Hladky [bd], P. Hristov [ah], M. Huang [q], T.J. Humanic [s], N. Hussain [ao], D. Hutter [am], D.S. Hwang [t], R. Ilkaev [cq], I. Ilkiv [bu], M. Inaba [dr], G.M. Innocenti [y], C. Ionita [ah], M. Ippolitov [cr], M. Irfan [r], M. Ivanov [co], V. Ivanov [cc], A. Jachołkowski [aa], P.M. Jacobs [br], C. Jahnke [dk], H.J. Jang [bl], M.A. Janik [dx], P.H.S.Y. Jayarathna [dm], C. Jena [ab], S. Jena [dm], R.T. Jimenez Bustamante [bg], P.G. Jones [ct], H. Jung [an], A. Jusko [ct], V. Kadyshevskiy [bj], S. Kalcher [am], P. Kalinak [bc], A. Kalweit [ah], J. Kamin [aw], J.H. Kang [eb], V. Kaplin [bt], S. Kar [dv], A. Karasu Uysal [bm], O. Karavichev [az], T. Karavicheva [az], E. Karpechev [az], U. Kebschull [av], R. Keidel [ec], D.L.D. Keijdener [ba], M.M. Khan [r,3], P. Khan [cs], S.A. Khan [dv], A. Khanzadeev [cc], Y. Kharlov [dd], B. Kileng [ai], B. Kim [eb], D.W. Kim [bl,an], D.J. Kim [dn], J.S. Kim [an], M. Kim [an], M. Kim [eb], S. Kim [t], T. Kim [eb], S. Kirsch [am], I. Kisel [am], S. Kiselev [bb], A. Kisiel [dx], G. Kiss [dz], J.L. Klay [f], J. Klein [ck], C. Klein-Bösing [ax], A. Kluge [ah], M.L. Knichel [co], A.G. Knospe [di], C. Kobdaj [df,ah], M. Kofarago [ah], M.K. Köhler [co], T. Kollegger [am], A. Kolojvari [du], V. Kondratiev [du], N. Kondratyeva [bt], A. Konevskikh [az], V. Kovalenko [du], M. Kowalski [dh], S. Kox [bo], G. Koyithatta Meethaleveedu [ar], J. Kral [dn], I. Králik [bc], A. Kravčáková [al], M. Krelina [ak], M. Kretz [am], M. Krivda [ct,bc], F. Krizek [ca], E. Kryshen [ah], M. Krzewicki [co,am], V. Kučera [ca], Y. Kucheriaev [cr,2], T. Kugathasan [ah], C. Kuhn [ay], P.G. Kuijer [by], I. Kulakov [aw], J. Kumar [ar], P. Kurashvili [bu], A. Kurepin [az], A.B. Kurepin [az], A. Kuryakin [cq], S. Kushpil [ca], M.J. Kweon [at,ck], Y. Kwon [eb], P. Ladron de Guevara [bg], C. Lagana Fernandes [dk], I. Lakomov [au], R. Langoy [dw], C. Lara [av], A. Lardeux [de], A. Lattuca [y], S.L. La Pointe [ba,dc], P. La Rocca [aa], R. Lea [x], L. Leardini [ck], G.R. Lee [ct], I. Legrand [ah], J. Lehnert [aw], R.C. Lemmon [bz], V. Lenti [cv], E. Leogrande [ba], M. Leoncino [y], I. León Monzón [dj], P. Lévai [dz], S. Li [g,bn], J. Lien [dw], R. Lietava [ct], S. Lindal [u], V. Lindenstruth [am], C. Lippmann [co], M.A. Lisa [s], H.M. Ljunggren [af], D.F. Lodato [ba], P.I. Loenne [q], V.R. Loggins [dy], V. Loginov [bt], D. Lohner [ck], C. Loizides [br], X. Lopez [bn], E. López Torres [i], X.-G. Lu [ck], P. Luettig [aw], M. Lunardon [ab], G. Luparello [ba,x], R. Ma [ea], A. Maevskaya [az], M. Mager [ah], D.P. Mahapatra [be], S.M. Mahmood [u], A. Maire [ck,ay], R.D. Majka [ea], M. Malaev [cc], I. Maldonado Cervantes [bg], L. Malinina [bj,4], D. Mal'Kevich [bb], P. Malzacher [co], A. Mamonov [cq], L. Manceau [dc], V. Manko [cr], F. Manso [bn], V. Manzari [cv], M. Marchisone [bn,y], J. Mareš [bd], G.V. Margagliotti [x], A. Margotti [cw], A. Marín [co], C. Markert [di], M. Marquard [aw], I. Martashvili [dp], N.A. Martin [co], P. Martinengo [ah], M.I. Martínez [b], G. Martínez García [de], J. Martin Blanco [de], Y. Martynov [c], A. Mas [de], S. Masciocchi [co], M. Masera [y], A. Masoni [cx], L. Massacrier [de], A. Mastroserio [ae], A. Matyja [dh], C. Mayer [dh], J. Mazer [dp], M.A. Mazzoni [da], F. Meddi [v], A. Menchaca-Rocha [bh], J. Mercado Pérez [ck], M. Meres [aj], Y. Miake [dr], K. Mikhaylov [bj,bb], L. Milano [ah], J. Milosevic [u,5], A. Mischke [ba], A.N. Mishra [as], D. Miśkowiec [co], J. Mitra [dv], C.M. Mitu [bf], J. Mlynarz [dy], N. Mohammadi [ba], B. Mohanty [bw,dv], L. Molnar [ay], L. Montaño Zetina [k], E. Montes [j], M. Morando [ab], D.A. Moreira De Godoy [dk], S. Moretto [ab], A. Morreale [de], A. Morsch [ah], V. Muccifora [bp], E. Mudnic [dg], D. Mühlheim [ax], S. Muhuri [dv], M. Mukherjee [dv], H. Müller [ah], M.G. Munhoz [dk], S. Murray [cg], L. Musa [ah], J. Musinsky [bc], B.K. Nandi [ar], R. Nania [cw], E. Nappi [cv], C. Nattrass [dp], K. Nayak [bw], T.K. Nayak [dv], S. Nazarenko [cq], A. Nedosekin [bb], M. Nicassio [co], M. Niculescu [ah,bf], B.S. Nielsen [bx], S. Nikolaev [cr], S. Nikulin [cr], V. Nikulin [cc], B.S. Nilsen [cd], F. Noferini [l,cw], P. Nomokonov [bj], G. Nooren [ba], J. Norman [do], A. Nyanin [cr], J. Nystrand [q], H. Oeschler [ck], S. Oh [ea], S.K. Oh [bk,an,6], A. Okatan [bm], L. Olah [dz], J. Oleniacz [dx], A.C. Oliveira Da Silva [dk], J. Onderwaater [co], C. Oppedisano [dc], A. Ortiz Velasquez [bg,af], A. Oskarsson [af], J. Otwinowski [dh,co], K. Oyama [ck], M. Ozdemir [aw], P. Sahoo [as], Y. Pachmayer [ck], M. Pachr [ak], P. Pagano [ac], G. Paić [bg], F. Painke [am], C. Pajares [p], S.K. Pal [dv], A. Palmeri [cy], D. Pant [ar], V. Papikyan [a], G.S. Pappalardo [cy], P. Pareek [as], W.J. Park [co], S. Parmar [ce], A. Passfeld [ax], D.I. Patalakha [dd], V. Paticchio [cv], B. Paul [cs], T. Pawlak [dx], T. Peitzmann [ba], H. Pereira Da Costa [n], E. Pereira De Oliveira Filho [dk], D. Peresunko [cr], C.E. Pérez Lara [by], A. Pesci [cw], V. Peskov [aw], Y. Pestov [e], V. Petráček [ak], M. Petran [ak], M. Petris [bv], M. Petrovici [bv], C. Petta [aa], S. Piano [db], M. Pikna [aj], P. Pillot [de], O. Pinazza [cw,ah], L. Pinsky [dm], D.B. Piyarathna [dm], M. Płoskoń [br], M. Planinic [ds,cp], J. Pluta [dx], S. Pochybova [dz], P.L.M. Podesta-Lerma [dj], M.G. Poghosyan [cd,ah], E.H.O. Pohjoisaho [ap],

B. Polichtchouk [dd], N. Poljak [cp,ds], A. Pop [bv], S. Porteboeuf-Houssais [bn], J. Porter [br], B. Potukuchi [ch], S.K. Prasad [dy,d], R. Preghenella [cw,l], F. Prino [dc], C.A. Pruneau [dy], I. Pshenichnov [az], G. Puddu [w], P. Pujahari [dy], V. Punin [cq], J. Putschke [dy], H. Qvigstad [u], A. Rachevski [db], S. Raha [d], J. Rak [dn], A. Rakotozafindrabe [n], L. Ramello [ad], R. Raniwala [ci], S. Raniwala [ci], S.S. Räsänen [ap], B.T. Rascanu [aw], D. Rathee [ce], A.W. Rauf [o], V. Razazi [w], K.F. Read [dp], J.S. Real [bo], K. Redlich [bu,7], R.J. Reed [dy,ea], A. Rehman [q], P. Reichelt [aw], M. Reicher [ba], F. Reidt [ah], R. Renfordt [aw], A.R. Reolon [bp], A. Reshetin [az], F. Rettig [am], J.-P. Revol [ah], K. Reygers [ck], V. Riabov [cc], R.A. Ricci [bq], T. Richert [af], M. Richter [u], P. Riedler [ah], W. Riegler [ah], F. Riggi [aa], A. Rivetti [dc], E. Rocco [ba], M. Rodríguez Cahuantzi [b], A. Rodriguez Manso [by], K. Røed [u], E. Rogochaya [bj], S. Rohni [ch], D. Rohr [am], D. Röhrich [q], R. Romita [bz,do], F. Ronchetti [bp], L. Ronflette [de], P. Rosnet [bn], A. Rossi [ah], F. Roukoutakis [cf], A. Roy [as], C. Roy [ay], P. Roy [cs], A.J. Rubio Montero [j], R. Rui [x], R. Russo [y], E. Ryabinkin [cr], Y. Ryabov [cc], A. Rybicki [dh], S. Sadovsky [dd], K. Šafařík [ah], B. Sahlmuller [aw], R. Sahoo [as], P.K. Sahu [be], J. Saini [dv], S. Sakai [bp,br], C.A. Salgado [p], J. Salzwedel [s], S. Sambyal [ch], V. Samsonov [cc], X. Sanchez Castro [ay], F.J. Sánchez Rodríguez [dj], L. Šándor [bc], A. Sandoval [bh], M. Sano [dr], G. Santagati [aa], D. Sarkar [dv], E. Scapparone [cw], F. Scarlassara [ab], R.P. Scharenberg [cm], C. Schiaua [bv], R. Schicker [ck], C. Schmidt [co], H.R. Schmidt [ag], S. Schuchmann [aw], J. Schukraft [ah], M. Schulc [ak], T. Schuster [ea], Y. Schutz [de,ah], K. Schwarz [co], K. Schweda [co], G. Scioli [z], E. Scomparin [dc], R. Scott [dp], G. Segato [ab], J.E. Seger [cd], Y. Sekiguchi [dq], I. Selyuzhenkov [co], J. Seo [cn], E. Serradilla [j,bh], A. Sevcenco [bf], A. Shabetai [de], G. Shabratova [bj], R. Shahoyan [ah], A. Shangaraev [dd], N. Sharma [dp], S. Sharma [ch], K. Shigaki [aq], K. Shtejer [y,i], Y. Sibiriak [cr], S. Siddhanta [cx], T. Siemiarczuk [bu], D. Silvermyr [cb], C. Silvestre [bo], G. Simatovic [ds], R. Singaraju [dv], R. Singh [ch], S. Singha [dv,bw], V. Singhal [dv], B.C. Sinha [dv], T. Sinha [cs], B. Sitar [aj], M. Sitta [ad], T.B. Skaali [u], K. Skjerdal [q], M. Slupecki [dn], N. Smirnov [ea], R.J.M. Snellings [ba], C. Søgaard [af], R. Soltz [bs], J. Song [cn], M. Song [eb], F. Soramel [ab], S. Sorensen [dp], M. Spacek [ak], E. Spiriti [bp], I. Sputowska [dh], M. Spyropoulou-Stassinaki [cf], B.K. Srivastava [cm], J. Stachel [ck], I. Stan [bf], G. Stefanek [bu], M. Steinpreis [s], E. Stenlund [af], G. Steyn [bi], J.H. Stiller [ck], D. Stocco [de], M. Stolpovskiy [dd], P. Strmen [aj], A.A.P. Suaide [dk], T. Sugitate [aq], C. Suire [au], M. Suleymanov [o], R. Sultanov [bb], M. Šumbera [ca], T. Susa [cp], T.J.M. Symons [br], A. Szabo [aj], A. Szanto de Toledo [dk], I. Szarka [aj], A. Szczepankiewicz [ah], M. Szymanski [dx], J. Takahashi [dl], M.A. Tangaro [ae], J.D. Tapia Takaki [au,8], A. Tarantola Peloni [aw], A. Tarazona Martinez [ah], M.G. Tarzila [bv], A. Tauro [ah], G. Tejeda Muñoz [b], A. Telesca [ah], C. Terrevoli [w], J. Thäder [co], D. Thomas [ba], R. Tieulent [dt], A.R. Timmins [dm], A. Toia [aw,cz], V. Trubnikov [c], W.H. Trzaska [dn], T. Tsuji [dq], A. Tumkin [cq], R. Turrisi [cz], T.S. Tveter [u], K. Ullaland [q], A. Uras [dt], G.L. Usai [w], M. Vajzer [ca], M. Vala [bc,bj], L. Valencia Palomo [bn], S. Vallero [y,ck], P. Vande Vyvre [ah], J. Van Der Maarel [ba], J.W. Van Hoorne [ah], M. van Leeuwen [ba], A. Vargas [b], M. Vargyas [dn], R. Varma [ar], M. Vasileiou [cf], A. Vasiliev [cr], V. Vechernin [du], M. Veldhoen [ba], A. Velure [q], M. Venaruzzo [x,bq], E. Vercellin [y], S. Vergara Limón [b], R. Vernet [h], M. Verweij [dy], L. Vickovic [dg], G. Viesti [ab], J. Viinikainen [dn], Z. Vilakazi [bi], O. Villalobos Baillie [ct], A. Vinogradov [cr], L. Vinogradov [du], Y. Vinogradov [cq], T. Virgili [ac], Y.P. Viyogi [dv], A. Vodopyanov [bj], M.A. Völkl [ck], K. Voloshin [bb], S.A. Voloshin [dy], G. Volpe [ah], B. von Haller [ah], I. Vorobyev [du], D. Vranic [co,ah], J. Vrláková [al], B. Vulpescu [bn], A. Vyushin [cq], B. Wagner [q], J. Wagner [co], V. Wagner [ak], M. Wang [g,de], Y. Wang [ck], D. Watanabe [dr], M. Weber [ah,dm], J.P. Wessels [ax], U. Westerhoff [ax], J. Wiechula [ag], J. Wikne [u], M. Wilde [ax], G. Wilk [bu], J. Wilkinson [ck], M.C.S. Williams [cw], B. Windelband [ck], M. Winn [ck], C.G. Yaldo [dy], Y. Yamaguchi [dq], H. Yang [ba], P. Yang [g], S. Yang [q], S. Yano [aq], S. Yasnopolskiy [cr], J. Yi [cn], Z. Yin [g], I.-K. Yoo [cn], I. Yushmanov [cr], V. Zaccolo [bx], C. Zach [ak], A. Zaman [o], C. Zampolli [cw], S. Zaporozhets [bj], A. Zarochentsev [du], P. Závada [bd], N. Zaviyalov [cq], H. Zbroszczyk [dx], I.S. Zgura [bf], M. Zhalov [cc], H. Zhang [g], X. Zhang [g,br], Y. Zhang [g], C. Zhao [u], N. Zhigareva [bb], D. Zhou [g], F. Zhou [g], Y. Zhou [ba], Zhuo Zhou [q], H. Zhu [g], J. Zhu [g], X. Zhu [g], A. Zichichi [l,z], A. Zimmermann [ck], M.B. Zimmermann [ax,ah], G. Zinovjev [c], Y. Zoccarato [dt], M. Zyzak [aw]

[a] *A.I. Alikhanyan National Science Laboratory (Yerevan Physics Institute) Foundation, Yerevan, Armenia*
[b] *Benemérita Universidad Autónoma de Puebla, Puebla, Mexico*
[c] *Bogolyubov Institute for Theoretical Physics, Kiev, Ukraine*
[d] *Bose Institute, Department of Physics and Centre for Astroparticle Physics and Space Science (CAPSS), Kolkata, India*
[e] *Budker Institute for Nuclear Physics, Novosibirsk, Russia*
[f] *California Polytechnic State University, San Luis Obispo, CA, United States*
[g] *Central China Normal University, Wuhan, China*
[h] *Centre de Calcul de l'IN2P3, Villeurbanne, France*
[i] *Centro de Aplicaciones Tecnológicas y Desarrollo Nuclear (CEADEN), Havana, Cuba*
[j] *Centro de Investigaciones Energéticas Medioambientales y Tecnológicas (CIEMAT), Madrid, Spain*
[k] *Centro de Investigación y de Estudios Avanzados (CINVESTAV), Mexico City and Mérida, Mexico*
[l] *Centro Fermi – Museo Storico della Fisica e Centro Studi e Ricerche "Enrico Fermi", Rome, Italy*

[m] Chicago State University, Chicago, USA
[n] Commissariat à l'Energie Atomique, IRFU, Saclay, France
[o] COMSATS Institute of Information Technology (CIIT), Islamabad, Pakistan
[p] Departamento de Física de Partículas and IGFAE, Universidad de Santiago de Compostela, Santiago de Compostela, Spain
[q] Department of Physics and Technology, University of Bergen, Bergen, Norway
[r] Department of Physics, Aligarh Muslim University, Aligarh, India
[s] Department of Physics, Ohio State University, Columbus, OH, United States
[t] Department of Physics, Sejong University, Seoul, South Korea
[u] Department of Physics, University of Oslo, Oslo, Norway
[v] Dipartimento di Fisica dell'Università 'La Sapienza' and Sezione INFN Rome, Italy
[w] Dipartimento di Fisica dell'Università and Sezione INFN, Cagliari, Italy
[x] Dipartimento di Fisica dell'Università and Sezione INFN, Trieste, Italy
[y] Dipartimento di Fisica dell'Università and Sezione INFN, Turin, Italy
[z] Dipartimento di Fisica e Astronomia dell'Università and Sezione INFN, Bologna, Italy
[aa] Dipartimento di Fisica e Astronomia dell'Università and Sezione INFN, Catania, Italy
[ab] Dipartimento di Fisica e Astronomia dell'Università and Sezione INFN, Padova, Italy
[ac] Dipartimento di Fisica 'E.R. Caianiello' dell'Università and Gruppo Collegato INFN, Salerno, Italy
[ad] Dipartimento di Scienze e Innovazione Tecnologica dell'Università del Piemonte Orientale and Gruppo Collegato INFN, Alessandria, Italy
[ae] Dipartimento Interateneo di Fisica 'M. Merlin' and Sezione INFN, Bari, Italy
[af] Division of Experimental High Energy Physics, University of Lund, Lund, Sweden
[ag] Eberhard Karls Universität Tübingen, Tübingen, Germany
[ah] European Organization for Nuclear Research (CERN), Geneva, Switzerland
[ai] Faculty of Engineering, Bergen University College, Bergen, Norway
[aj] Faculty of Mathematics, Physics and Informatics, Comenius University, Bratislava, Slovakia
[ak] Faculty of Nuclear Sciences and Physical Engineering, Czech Technical University in Prague, Prague, Czech Republic
[al] Faculty of Science, P.J. Šafárik University, Košice, Slovakia
[am] Frankfurt Institute for Advanced Studies, Johann Wolfgang Goethe-Universität Frankfurt, Frankfurt, Germany
[an] Gangneung-Wonju National University, Gangneung, South Korea
[ao] Gauhati University, Department of Physics, Guwahati, India
[ap] Helsinki Institute of Physics (HIP), Helsinki, Finland
[aq] Hiroshima University, Hiroshima, Japan
[ar] Indian Institute of Technology Bombay (IIT), Mumbai, India
[as] Indian Institute of Technology Indore, Indore (IITI), India
[at] Inha University, Incheon, South Korea
[au] Institut de Physique Nucléaire d'Orsay (IPNO), Université Paris-Sud, CNRS-IN2P3, Orsay, France
[av] Institut für Informatik, Johann Wolfgang Goethe-Universität Frankfurt, Frankfurt, Germany
[aw] Institut für Kernphysik, Johann Wolfgang Goethe-Universität Frankfurt, Frankfurt, Germany
[ax] Institut für Kernphysik, Westfälische Wilhelms-Universität Münster, Münster, Germany
[ay] Institut Pluridisciplinaire Hubert Curien (IPHC), Université de Strasbourg, CNRS-IN2P3, Strasbourg, France
[az] Institute for Nuclear Research, Academy of Sciences, Moscow, Russia
[ba] Institute for Subatomic Physics of Utrecht University, Utrecht, Netherlands
[bb] Institute for Theoretical and Experimental Physics, Moscow, Russia
[bc] Institute of Experimental Physics, Slovak Academy of Sciences, Košice, Slovakia
[bd] Institute of Physics, Academy of Sciences of the Czech Republic, Prague, Czech Republic
[be] Institute of Physics, Bhubaneswar, India
[bf] Institute of Space Science (ISS), Bucharest, Romania
[bg] Instituto de Ciencias Nucleares, Universidad Nacional Autónoma de México, Mexico City, Mexico
[bh] Instituto de Física, Universidad Nacional Autónoma de México, Mexico City, Mexico
[bi] iThemba LABS, National Research Foundation, Somerset West, South Africa
[bj] Joint Institute for Nuclear Research (JINR), Dubna, Russia
[bk] Konkuk University, Seoul, South Korea
[bl] Korea Institute of Science and Technology Information, Daejeon, South Korea
[bm] KTO Karatay University, Konya, Turkey
[bn] Laboratoire de Physique Corpusculaire (LPC), Clermont Université, Université Blaise Pascal, CNRS-IN2P3, Clermont-Ferrand, France
[bo] Laboratoire de Physique Subatomique et de Cosmologie, Université Grenoble-Alpes, CNRS-IN2P3, Grenoble, France
[bp] Laboratori Nazionali di Frascati, INFN, Frascati, Italy
[bq] Laboratori Nazionali di Legnaro, INFN, Legnaro, Italy
[br] Lawrence Berkeley National Laboratory, Berkeley, CA, United States
[bs] Lawrence Livermore National Laboratory, Livermore, CA, United States
[bt] Moscow Engineering Physics Institute, Moscow, Russia
[bu] National Centre for Nuclear Studies, Warsaw, Poland
[bv] National Institute for Physics and Nuclear Engineering, Bucharest, Romania
[bw] National Institute of Science Education and Research, Bhubaneswar, India
[bx] Niels Bohr Institute, University of Copenhagen, Copenhagen, Denmark
[by] Nikhef, National Institute for Subatomic Physics, Amsterdam, Netherlands
[bz] Nuclear Physics Group, STFC Daresbury Laboratory, Daresbury, United Kingdom
[ca] Nuclear Physics Institute, Academy of Sciences of the Czech Republic, Řež u Prahy, Czech Republic
[cb] Oak Ridge National Laboratory, Oak Ridge, TN, United States
[cc] Petersburg Nuclear Physics Institute, Gatchina, Russia
[cd] Physics Department, Creighton University, Omaha, NE, United States
[ce] Physics Department, Panjab University, Chandigarh, India
[cf] Physics Department, University of Athens, Athens, Greece
[cg] Physics Department, University of Cape Town, Cape Town, South Africa
[ch] Physics Department, University of Jammu, Jammu, India
[ci] Physics Department, University of Rajasthan, Jaipur, India
[cj] Physik Department, Technische Universität München, Munich, Germany
[ck] Physikalisches Institut, Ruprecht-Karls-Universität Heidelberg, Heidelberg, Germany
[cl] Politecnico di Torino, Turin, Italy
[cm] Purdue University, West Lafayette, IN, United States

[cn] Pusan National University, Pusan, South Korea
[co] Research Division and ExtreMe Matter Institute EMMI, GSI Helmholtzzentrum für Schwerionenforschung, Darmstadt, Germany
[cp] Rudjer Bošković Institute, Zagreb, Croatia
[cq] Russian Federal Nuclear Center (VNIIEF), Sarov, Russia
[cr] Russian Research Centre Kurchatov Institute, Moscow, Russia
[cs] Saha Institute of Nuclear Physics, Kolkata, India
[ct] School of Physics and Astronomy, University of Birmingham, Birmingham, United Kingdom
[cu] Sección Física, Departamento de Ciencias, Pontificia Universidad Católica del Perú, Lima, Peru
[cv] Sezione INFN, Bari, Italy
[cw] Sezione INFN, Bologna, Italy
[cx] Sezione INFN, Cagliari, Italy
[cy] Sezione INFN, Catania, Italy
[cz] Sezione INFN, Padova, Italy
[da] Sezione INFN, Rome, Italy
[db] Sezione INFN, Trieste, Italy
[dc] Sezione INFN, Turin, Italy
[dd] SSC IHEP of NRC Kurchatov Institute, Protvino, Russia
[de] SUBATECH, Ecole des Mines de Nantes, Université de Nantes, CNRS-IN2P3, Nantes, France
[df] Suranaree University of Technology, Nakhon Ratchasima, Thailand
[dg] Technical University of Split FESB, Split, Croatia
[dh] The Henryk Niewodniczanski Institute of Nuclear Physics, Polish Academy of Sciences, Cracow, Poland
[di] The University of Texas at Austin, Physics Department, Austin, TX, USA
[dj] Universidad Autónoma de Sinaloa, Culiacán, Mexico
[dk] Universidade de São Paulo (USP), São Paulo, Brazil
[dl] Universidade Estadual de Campinas (UNICAMP), Campinas, Brazil
[dm] University of Houston, Houston, TX, United States
[dn] University of Jyväskylä, Jyväskylä, Finland
[do] University of Liverpool, Liverpool, United Kingdom
[dp] University of Tennessee, Knoxville, TN, United States
[dq] University of Tokyo, Tokyo, Japan
[dr] University of Tsukuba, Tsukuba, Japan
[ds] University of Zagreb, Zagreb, Croatia
[dt] Université de Lyon, Université Lyon 1, CNRS/IN2P3, IPN-Lyon, Villeurbanne, France
[du] V. Fock Institute for Physics, St. Petersburg State University, St. Petersburg, Russia
[dv] Variable Energy Cyclotron Centre, Kolkata, India
[dw] Vestfold University College, Tonsberg, Norway
[dx] Warsaw University of Technology, Warsaw, Poland
[dy] Wayne State University, Detroit, MI, United States
[dz] Wigner Research Centre for Physics, Hungarian Academy of Sciences, Budapest, Hungary
[ea] Yale University, New Haven, CT, United States
[eb] Yonsei University, Seoul, South Korea
[ec] Zentrum für Technologietransfer und Telekommunikation (ZTT), Fachhochschule Worms, Worms, Germany

[1] St. Petersburg State Polytechnical University.
[2] Deceased.
[3] Department of Applied Physics, Aligarh Muslim University, Aligarh, India.
[4] M.V. Lomonosov Moscow State University, D.V. Skobeltsyn Institute of Nuclear Physics, Moscow, Russia.
[5] University of Belgrade, Faculty of Physics and "Vinča" Institute of Nuclear Sciences, Belgrade, Serbia.
[6] Permanent address: Konkuk University, Seoul, Korea.
[7] Institute of Theoretical Physics, University of Wroclaw, Wroclaw, Poland.
[8] University of Kansas, Lawrence, KS, United States.

Update

Physics Letters B

Volume 763, Issue , 10 December 2016, Page 507–509

DOI: https://doi.org/10.1016/j.physletb.2016.10.004

Physics Letters B 763 (2016) 507–509

Contents lists available at ScienceDirect

Physics Letters B

www.elsevier.com/locate/physletb

Corrigendum

Corrigendum to "Measurement of electrons from beauty hadron decays in pp collisions at $\sqrt{s} = 7$ TeV" [Phys. Lett. B 721 (1–3) (2013) 13–23] and "Beauty production in pp collisions at $\sqrt{s} = 2.76$ TeV measured via semi-electronic decays" [Phys. Lett. B 738 (2014) 97–108]

ALICE Collaboration

ARTICLE INFO

Article history:
Available online 25 October 2016

We have identified a bias in the measurement of electrons from beauty-hadron decays in pp collisions at center-of-mass energies $\sqrt{s} = 2.76$ TeV [1] and $\sqrt{s} = 7$ TeV [2]. The efficiency corrections were evaluated using a Monte Carlo simulation, based on PYTHIA as described in [1,2]. When calculating the impact parameter (d_0) cut efficiency for the charm-hadron decay electrons, we did not consider the difference between the impact parameter distributions using the measured D-meson p_T distribution and the one from Monte Carlo.

For weakly decaying hadrons with sufficiently high transverse momentum (p_T), the impact parameter distribution of the daughter particle at a given p_T depends very weakly on the transverse momentum of the mother hadrons. However, at low momentum the impact parameter distribution of the decay particles depends on the momentum distribution of the mother hadrons. Due to the harder p_T spectra of charm hadrons in the Monte Carlo simulation [1,2] compared to the measured ones [3,4], the d_0 cut efficiency of decay electrons was biased towards larger values. Since the background was subtracted from the raw inclusive electron yield after applying the d_0 cut, the charm-hadron decay background was overestimated.

We have now computed the d_0 distribution of electrons from charm-hadron decays using a Monte Carlo and weighting each electron by the ratio $(dN/dp_T)^{\text{measured}}/(dN/dp_T)^{\text{MC}}$. $(dN/dp_T)^{\text{measured}}$ and $(dN/dp_T)^{\text{MC}}$ are the production yields evaluated at the p_T of the mother charm-hadron of the electron, as obtained from data [3,4] and in the Monte Carlo simulations [1,2], respectively. In such a way, the measured mother p_T spectra are propagated to the impact parameter cut efficiency calculation for the daughter electrons.

Table 1
Effect of the corrected treatment of the D-meson p_T distribution on the d_0 cut efficiency for electrons from charm-hadron decays (ϵ_{d_0}) and the resulting yield of signal electrons (dN^{signal}/dp_T).

7 TeV pp collisions			
p_T interval (GeV/c)	1–2	2–3	3–8
$\epsilon_{d_0}^{\text{updated}}/\epsilon_{d_0}^{\text{previous}}$	0.56–0.60	0.60–0.70	0.70–0.85
$(dN^{\text{signal}}/dp_T)^{\text{updated}}/(dN^{\text{signal}}/dp_T)^{\text{previous}}$	1.6–1.4	1.3–1.2	< 1.1
2.76 TeV pp collisions			
p_T interval (GeV/c)	1–2	2–3	3–8
$\epsilon_{d_0}^{\text{updated}}/\epsilon_{d_0}^{\text{previous}}$	0.74–0.77	0.77–0.85	0.85–0.94
$(dN^{\text{signal}}/dp_T)^{\text{updated}}/(dN^{\text{signal}}/dp_T)^{\text{previous}}$	1.4–1.3	1.2–1.1	< 1.1

The new value of the d_0 cut efficiency ($\epsilon_{d_0}^{\text{updated}}$) of electrons from charm-hadron decays is significantly smaller than that previously evaluated ($\epsilon_{d_0}^{\text{previous}}$) as summarized in Table 1.

In Fig. 1, the raw electron yield, as well as the non-beauty electron background yield, which is subtracted in the analysis, are shown after the application of the track selection criteria. Compared to Fig. 3 in [2], the yield of electrons from charm-hadron decays is smaller by the factor $\epsilon_{d_0}^{\text{updated}}/\epsilon_{d_0}^{\text{previous}}$ given in Table 1. The corresponding yield of beauty-signal electrons (dN^{signal}/dp_T) increases as listed in Table 1. For pp collisions at $\sqrt{s} = 2.76$ TeV, where a similar bias was present, the same procedure has been applied and the correct distributions are shown in Fig. 2 (to be compared with Fig. 2 in [1]). Numerical values of the implication for the d_0 cut efficiency are given in Table 1.

The uncertainty on the d_0 efficiency was evaluated by propagating the statistical and systematic uncertainties of the charm-hadron p_T distributions in [3] to the measurements discussed in this corrigendum. The uncertainty was added in quadrature as an independent contribution to the total systematic uncertainty.

DOIs of original articles: http://dx.doi.org/10.1016/j.physletb.2013.01.069, http://dx.doi.org/10.1016/j.physletb.2014.09.026.

http://dx.doi.org/10.1016/j.physletb.2016.10.004
0370-2693

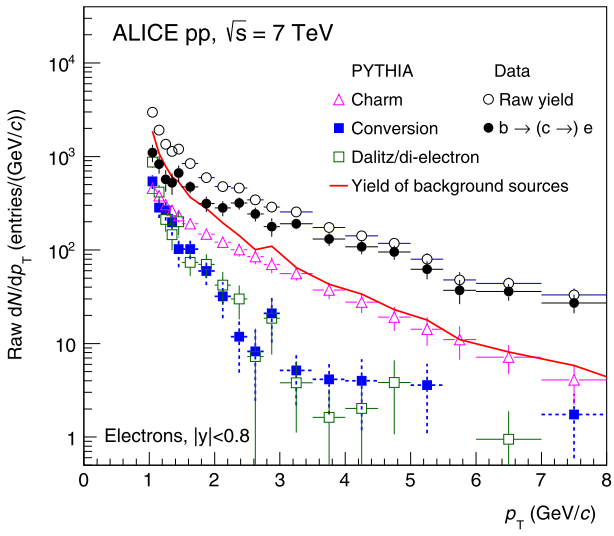

Fig. 1. This figure replaces Fig. 3 from [2]. Caption is the same as Fig. 3 from [2].

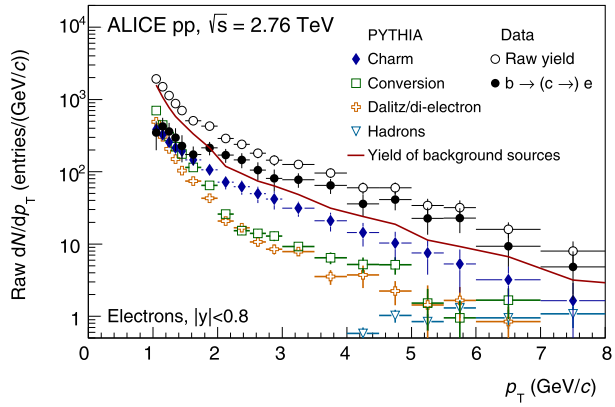

Fig. 2. This figure replaces Fig. 2 from [1]. Caption is the same as Fig. 2 from [1].

Table 2
Summary of the updated cross sections.

Cross sections at 7 TeV pp collisions	
Visible $\sigma_{b\to e}$	9.03 ± 0.50 (stat) $^{+2.72}_{-2.73}$ (sys) ± 0.32 (norm) μb
$d\sigma_{b\bar{b}}/dy$	57.7 ± 3.2 (stat) $^{+17.4}_{-17.4}$ (sys) $^{+1.4}_{-2.3}$ (extr) ± 2.0 (norm) μb
$\sigma_{b\bar{b}}$	383 ± 21 (stat) $^{+116}_{-116}$ (sys) $^{+10}_{-11}$ (extr) ± 13 (norm) ± 13 (br) μb
Weighted $\sigma_{b\bar{b}}$	322 ± 45 (stat) $^{+58}_{-62}$ (sys) $^{+8}_{-9}$ (extr) μb
$d\sigma_{c\bar{c}}/dy$	1.1 ± 0.2 (stat) $^{+0.6}_{-0.7}$ (sys) $^{+0.2}_{-0.1}$ (extr) mb
$\sigma_{c\bar{c}}$	9.7 ± 1.7 (stat) $^{+5.2}_{-5.6}$ (sys) $^{+3.4}_{-0.5}$ (extr) ± 0.4 (br) mb
Cross sections at 2.76 TeV pp collisions	
Visible $\sigma_{b\to e}$	4.33 ± 0.38 (stat) $^{+1.45}_{-1.75}$ (sys) ± 0.08 (norm) μb
$d\sigma_{b\bar{b}}/dy$	29.1 ± 2.6 (stat) $^{+9.8}_{-11.7}$ (sys) $^{+0.6}_{-0.8}$ (extr) ± 0.6 (norm) μb
$\sigma_{b\bar{b}}$	162 ± 14 (stat) $^{+55}_{-65}$ (sys) $^{+4}_{-4}$ (extr) ± 3 (norm) ± 6 (br) μb

The relative systematic uncertainties on the charm-hadron decay background increase by 3% (2%) at $p_T < 1.5$ GeV/c for 7 TeV (2.76 TeV) pp collisions. The change of the systematic uncertainties at higher p_T region is instead negligible. However, the amount of background decreases and as a consequence the total uncertainty on the beauty production measurement decreases.

The production cross sections were also corrected correspondingly. The integrated cross section of electrons from beauty hadron

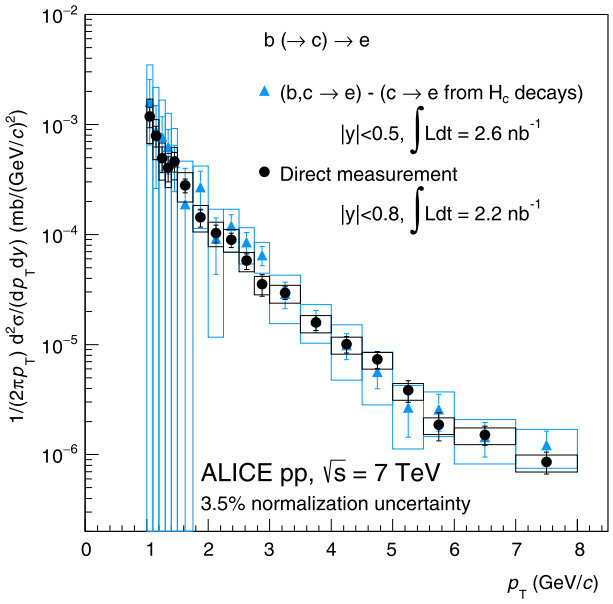

Fig. 3. This figure replaces Fig. 4 from [2]. Caption is the same as Fig. 4 from [2].

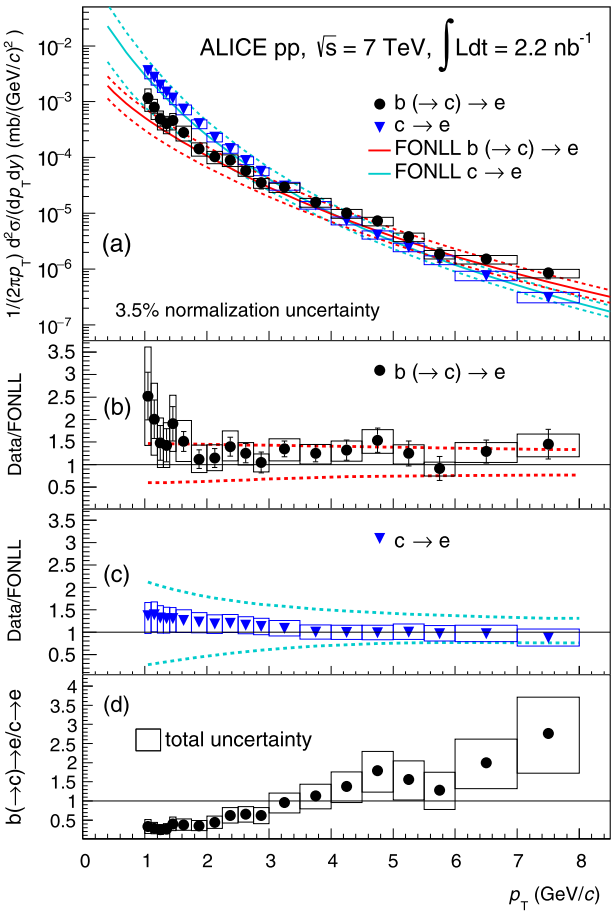

Fig. 4. This figure replaces Fig. 5 from [2]. Caption is the same as Fig. 5 from [2].

decays (visible $\sigma_{b\to e}$), the beauty production cross section per unit rapidity at mid-rapidity ($d\sigma_{b\bar{b}}/dy$) and the total cross section ($\sigma_{b\bar{b}}$) are summarized in Table 2. For 7 TeV pp collisions, the weighted average of this with the result of a previous measurement of

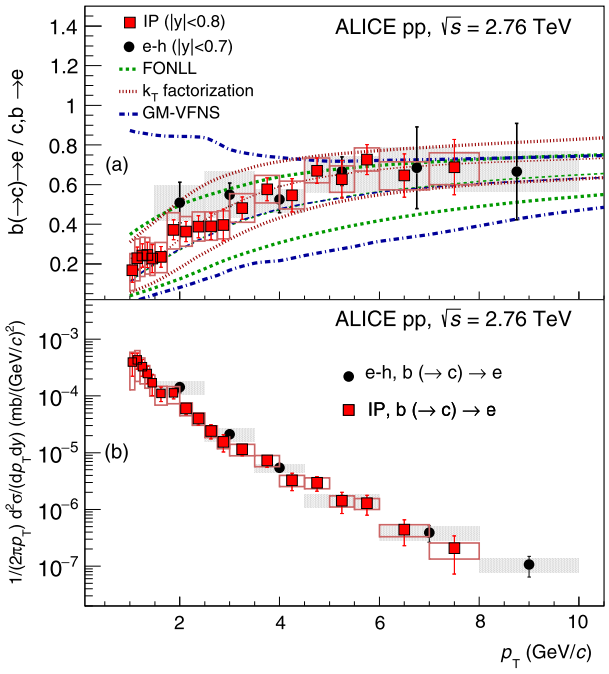

Fig. 5. This figure replaces Fig. 4 from [1]. Caption is the same as Fig. 4 from [1].

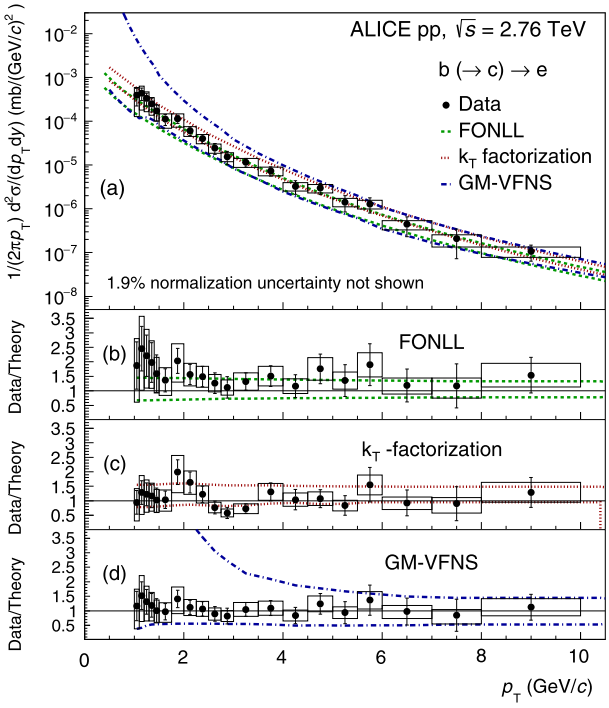

Fig. 6. This figure replaces Fig. 5 from [1]. Caption is the same as Fig. 5 from [1].

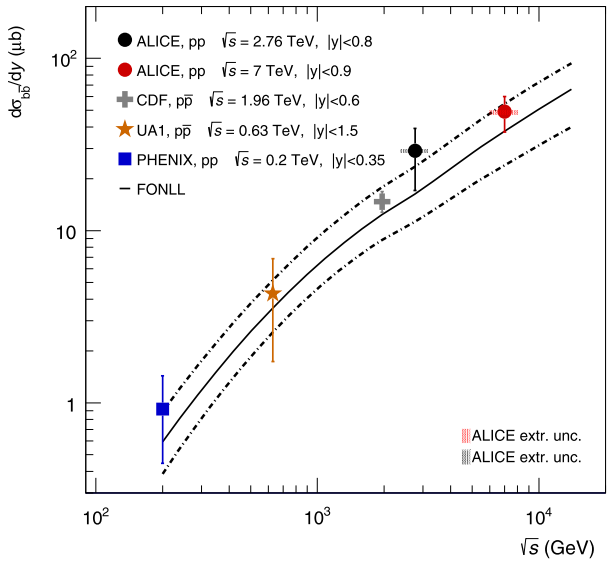

Fig. 7. This figure replaces Fig. 6 from [1]. Caption is the same as Fig. 6 from [1].

J/ψ mesons from beauty-hadron decays [5] is also updated. After subtracting the new cross section of the electrons from beauty-hadron decays from the measured cross section of the electrons from heavy-flavour hadron decays [6], the production cross section of electrons from charm-hadron decays was converted into a charm production cross section. The charm production cross section per unit rapidity at mid-rapidity ($d\sigma_{c\bar{c}}/dy$) and the total cross sections ($\sigma_{c\bar{c}}$) at $\sqrt{s} = 7$ TeV are also updated in Table 2. Since the corresponding quantity at $\sqrt{s} = 2.76$ TeV was not explicitly evaluated in [1], there is no corresponding entry in Table 2. All measured cross sections for 7 TeV (2.76 TeV) have an additional normalization uncertainty of 3.5% (1.9%) [7].

In Figs. 3, 4, 5, 6 and 7, we have updated accordingly the ALICE data points.

The main conclusion of the original papers remains valid: the data and predictions are consistent within the experimental and theoretical uncertainties.

References

[1] B. Abelev, et al., ALICE Collaboration, Phys. Lett. B 738 (2014) 97.
[2] B. Abelev, et al., ALICE Collaboration, Phys. Lett. B 721 (2013) 13.
[3] K. Aamodt, et al., ALICE Collaboration, J. High Energy Phys. 01 (2012) 128.
[4] B. Abelev, et al., ALICE Collaboration, J. High Energy Phys. 1207 (2012) 191, arXiv:1205.4007 [hep-ex].
[5] B. Abelev, et al., ALICE Collaboration, J. High Energy Phys. 11 (2012) 1.
[6] B. Abelev, et al., ALICE Collaboration, Phys. Rev. D 86 (2012) 112007, arXiv:1205.5423 [hep-ex].
[7] B. Abelev, et al., ALICE Collaboration, Eur. Phys. J. C 73 (2013) 1.